

INFORMATION TO USERS

This manuscript has been reproduced from the microfilm master. UMI films the text directly from the original or copy submitted. Thus, some thesis and dissertation copies are in typewriter face, while others may be from any type of computer printer.

The quality of this reproduction is dependent upon the quality of the copy submitted. Broken or indistinct print, colored or poor quality illustrations and photographs, print bleedthrough, substandard margins, and improper alignment can adversely affect reproduction.

In the unlikely event that the author did not send UMI a complete manuscript and there are missing pages, these will be noted. Also, if unauthorized copyright material had to be removed, a note will indicate the deletion.

Oversize materials (e.g., maps, drawings, charts) are reproduced by sectioning the original, beginning at the upper left-hand corner and continuing from left to right in equal sections with small overlaps. Each original is also photographed in one exposure and is included in reduced form at the back of the book.

Photographs included in the original manuscript have been reproduced xerographically in this copy. Higher quality 6" x 9" black and white photographic prints are available for any photographs or illustrations appearing in this copy for an additional charge. Contact UMI directly to order.

U·M·I

University Microfilms International
A Bell & Howell Information Company
300 North Zeeb Road, Ann Arbor, MI 48106-1346 USA
313/761-4700 800/521-0600

4-10-10

Order Number 1355173

Influence of pyrolysis conditions on macropore structure of char particles

Boissiere, François Patrice, M.S.

Rice University, 1993

U·M·I

300 N. Zeeb Rd.
Ann Arbor, MI 48106

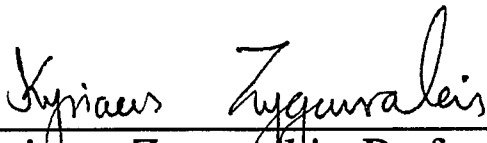
RICE UNIVERSITY

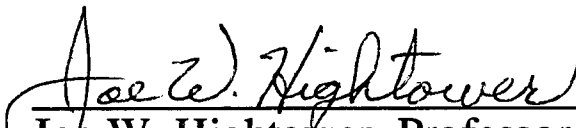
INFLUENCE OF PYROLYSIS CONDITIONS ON
MACROPORE
STRUCTURE OF CHAR PARTICLES

by
FRANÇOIS BOISSIERE

A THESIS SUBMITTED
IN PARTIAL FULFILLMENT OF THE
REQUIREMENTS FOR THE DEGREE
MASTER OF SCIENCE

APPROVED, THESIS COMMITTEE


Kyriacos Zygourakis, Professor
Chemical Engineering, Chairman


Joe W. Hightower, Professor
Chemical Engineering


Constantine Armeniades, Professor
Chemical Engineering

Houston, Texas
March, 1993

INFLUENCE OF PYROLYSIS CONDITIONS ON MACROPORE STRUCTURE OF CHAR PARTICLES

by

François BOISSIERE

ABSTRACT

A systematic analysis of the structure of char particles produced from an Illinois #6 coal was carried out. Coal particles were pyrolyzed in a hot-stage reactor under inert (N₂) and reactive (5% O₂ / 95% N₂) atmospheres at various heating rates (0.1, 1 and 10 °C/s) and final heat treatment temperatures (500 and 700 °C). Image analysis procedures were used to measure the size and macroporosity of the particles, and the surface area and size distribution of the macropores.

High heating rates and the addition of oxygen resulted in larger particle swelling and increased the macroporosity, the surface area and the fraction of large macropores with thin walls. Heat treatment temperatures had smaller effects on char particle structure. Our data confirm the strong effects of pyrolysis conditions on char reactivity during combustion in the diffusion-limited regime. They also provide the necessary parameters for char combustion models.

AKNOWLEDGEMENTS

Many people and organizations deserve special recognition for the influence they had on my graduate studies. They include:

- Dr. Zygourakis for his constant support throughout the course of my research. He was always understanding and ready to help me solving the different problems I faced in the past four years.

- Dr. Armeniades and Dr. Hightower for serving in my thesis committee.

- Andreas Matzakos and Ahmad Ismail have been wonderful and very helpfull labmates.

- ENSIGC, the department of Chemical Engineering and the foreign student advising office at Rice University without whom this would not have been possible.

- The U.S. Department of Energy (University Coal Research program) for supporting my project financially.

- My family and Pierre, Sam, Ellen, Jean-Luc, Amy, Brian, Pascale, Marie-Do, Patrick, Sylvie, Pierre and Antoine, my successive roommates, for their support and friendship.

All these persons should be thanked for making the past few years some of the best in my life.

TABLE OF CONTENTS

CHAPTER 1

INTRODUCTION AND STATEMENT OF

OBJECTIVES.....	1
1.1 COAL UTILIZATION.....	1
1.2 PHYSICAL PROPERTIES OF COAL.....	3
1.3 COAL PYROLYSIS.....	5
1.3.1 Devolatilization.....	5
1.3.2 Plasticity.....	7
1.3.3 Physicochemical Mechanisms of Pyrolysis.....	9
1.4 COAL COMBUSTION.....	11
1.4.1 Pore Surface Area and Reactivity.....	12
1.4.2 Environmental considerations.....	13
1.5 OBJECTIVES OF OUR STUDY.....	14
1.5.1 Effect of Pyrolysis Conditions on the Macropore Structure of Chars.....	14
1.5.2 Development of Experimental Techniques for Macropore Structure Analysis.....	17

CHAPTER 2

EXPERIMENTAL EQUIPMENT AND PROCEDURES.....	20
2.1 PYROLYSIS.....	20
2.1.1 Choice of coal.....	20
2.1.2 Particle size.....	21
2.1.3 Pyrolysis Reactor.....	21

2.1.4	Typical pyrolysis experiment.....	24
2.2	PARTICLE SWELLING DURING PYROLYSIS.....	26
2.3	MACROPORE STRUCTURE ANALYSIS.....	28
2.3.1	Preparation of the polished cross sections.....	28
2.3.2	Digital image acquisition.....	32
2.3.3	Image analysis.....	34
2.3.4	Measuring the Volume and Surface Area of Macropores.....	37
2.3.5	Macropore Size Distribution.....	38

CHAPTER 3

	PARTICLE SWELLING DURING PYROLYSIS.....	40
3.1	SOME QUALITATIVE OBSERVATIONS.....	40
3.2	PYROLYSIS CONDITIONS AND CHAR PARTICLE SIZE.....	43
3.3	PYROLYSIS CONDITIONS AND CHAR PARTICLE SHAPE..	51
3.4	HEATING RATE AND PARTICLE SIZE DISTRIBUTION.....	56
3.5	HTT AND PARTICLE SIZE DISTRIBUTION.....	59
3.6	OXYGEN ATMOSPHERE AND PARTICLE SIZE DISTRIBUTION.....	59

CHAPTER 4

	MACROPORE STRUCTURE ANALYSIS.....	65
4.1	PYROLYSIS CONDITIONS AND CHAR MACROPORE STRUCTURE.....	65

4.2 MACROPOROSITY.....	71
4.3 MACROPORE SURFACE AREA.....	74
4.4 PORE SIZE DISTRIBUTION.....	77

CHAPTER 5

CONCLUSIONS AND RECOMMENDATIONS FOR FUTURE WORK.....	90
5.1 MACROPORE STRUCTURE AND CHAR REACTIVITY DURING COMBUSTION.....	90
5.1.1 Effect of HTT on Char Reactivity.....	90
5.1.2 Effect of heating rate.....	91
5.1.3 Effect of oxygen.....	92
5.2 CONCLUSIONS.....	92
5.3 RECOMMENDATIONS FOR FUTURE WORK.....	94

LIST OF FIGURES

Figure 2.1:	Pyrolysis hot-stage reactor.....	23
Figure 2.2:	Schematic showing the video microscopy system for the hot-stage reactor.....	25
Figure 2.3:	Embedding of the particles.....	30
Figure 2.4:	Greyscale image of a coal particle cross-section.....	33
Figure 2.5:	Processing of the greyscale image.....	35
Figure 2.6:	Processing of the binary image.....	36
Figure 3.1:	Projected areas of particles before pyrolysis and after pyrolysis at HTT 700 °C without oxygen.....	44
Figure 3.2:	Projected areas of particles before pyrolysis and after pyrolysis at HTT 500 °C without oxygen.....	45
Figure 3.3:	Projected areas of particles pyrolysed at HTT of 500 °C.....	46
Figure 3.4:	Projected areas of particles pyrolysed at 10 °C/s and HTT of 700 °C.....	47
Figure 3.5:	Effect of pyrolysis conditions on average particle area equivalent radius.....	49
Figure 3.6:	Effect of pyrolysis conditions on swelling ratio.....	51
Figure 3.7:	Width and length distribution of 61 particles before pyrolysis.....	53
Figure 3.8:	Width and length distribution of 60 particles after pyrolysis at 0.1 °C/s, HTT 700 °C without oxygen.....	53

Figure 3.9:	Width and length distribution of 64 particles after pyrolysis at 1 °C/s, HTT 500 with 5% oxygen.....	54
Figure 3.10:	Width and length distribution of 176 particles after pyrolysis at 10 °C/s, HTT 700 °C with 5% oxygen.....	54
Figure 3.11:	Distribution of shape factors for the base case and pyrolysis at 10 °C/s, 700 °C HTT and 5% O ₂	55
Figure 3.12:	Particle size distribution after pyrolysis at HTT 700 °C, without O ₂ (0.1°C/s: 60 part., 1°C/s: 125 part.).....	57
Figure 3.13:	Particle size distribution after pyrolysis at HTT 700 °C without O ₂ (1 °C/s: 125 part., 10 °C/s 145 part.).....	57
Figure 3.14:	Particle size distribution after pyrolysis at HTT 500 °C without O ₂ (0.1 °C/s: 54 part., 1 °C/s: 106 part.).....	58
Figure 3.15:	Particle size distribution after pyrolysis at HTT 500 °C without O ₂ (1 °C/s: 106 part., 10 °C/s: 134 part.).....	58
Figure 3.16:	Particle size distribution after pyrolysis at 0.1 °C/s without O ₂ (HTT 500°C: 54 part., HTT 700°C: 60 part.).....	60
Figure 3.17:	Particle size distribution after pyrolysis at 1 °C/s without O ₂ (HTT 500°C: 106 part., HTT 700°C: 125 part.).....	60

Figure 3.18:	Particle size distribution after pyrolysis at 10 °C/s with 5%O ₂ (HTT 500°C: 120 part., HTT 700 °C: 176 part.).....	61
Figure 3.19:	Particle size distribution after pyrolysis at 10 °C/s without O ₂ (HTT 500°C: 134 part., HTT 700 °C: 145 part.).....	61
Figure 3.20:	Particle size distribution after pyrolysis at 1 °C/s and HTT 500 °C (0% O ₂ : 106 part., 5% O ₂ 64 part.).....	63
Figure 3.21:	Particle size distribution after pyrolysis at 10 °C/s and HTT 700 °C (0% O ₂ : 145 part., 5% O ₂ 176 part.).....	63
Figure 3.22:	Particle size distribution after pyrolysis at 10 °C/s with HTT 500 °C (0% O ₂ : 134 part., 5% O ₂ : 120 part.).....	64
Figure 3.23:	Particle size distribution after pyrolysis at HTT 500 °C with 5% O ₂ (1 °C/s: 64 part., 10 °C/s: 120 part.).....	64
Figure 4.1:	Cross sections of particles pyrolysed to an HTT of 700 °C without oxygen.....	67
Figure 4.2:	Cross-sections of particles pyrolysed at 1 °C/s and 10 °C/s without oxygen.....	68
Figure 4.3:	Cross-sections of particles pyrolysed at 1 °C/s and 10 °C/s at HTT of 500 °C.....	69
Figure 4.4:	Cross-sections of particles pyrolysed at 1 °C/s and 10 °C/s at HTT of 700 °C.....	70

Figure 4.5:	Effect of pyrolysis heating rate on macroporosity for two values of heat treatment temperature and two pyrolysis atmospheres.....	74
Figure 4.6:	Effect of pyrolysis conditions on specific macropore surface area, S_g	76
Figure 4.7:	Macropore distribution for heating rates of 0.1 °C/s and 1 °C/s.....	79
Figure 4.8:	Macropore size distribution for heating rate of 10 °C/s.....	80
Figure 4.9:	Effect of pyrolysis heating rate on macropore volume distribution.....	82
Figure 4.10:	Effect of heat treatment temperature on macropore volume distribution.....	83
Figure 4.11:	Effect of heat treatment temperature (HTT) and oxygen on macropore volume distribution.....	86
Figure 4.12:	Effect of oxygen on macropore size distribution.....	87
Figure 4.13:	Differences in macroporosity between the unbiased estimate and the value given by the stereological method.....	88
Figure 4.14:	Differences in specific macropore surface area between the unbiased estimate and the value given by the stereological method.....	89

LIST OF TABLES

Table 3.1:	Temperature Ranges for Coal Plasticity.....	41
Table 3.2:	Effect of Pyrolysis Conditions on the Size of Char Particles.....	48
Table 4.1:	Unbiased estimates from the 2D results.....	73
Table 4.2:	Values of R50.....	78
Table 4.3:	Porosity and surface area density from pore distributio.	85

CHAPTER 1

INTRODUCTION AND STATEMENT OF OBJECTIVES

1.1 COAL UTILIZATION

Coal is one of the oldest energy sources used on earth. One can find traces of coal mining 2000 years ago (Eavenson, 1939). The use of coal has been continuously increasing since then, replacing wood as the primary energy source. The peak in coal consumption occurred in the 19th century, when the industrial revolution was fueled on coal both through the growth of the steam engine and by the development of iron making. During the 20th century, the development of new energy sources (oil, natural gas, nuclear energy, and on a smaller scale, solar, geothermal, hydro-electric and other alternative energy sources) has stopped this hegemony (Judkins, Fulkerson et al., 1991).

We have large quantities of coal on earth. Coal reserves of $1,026.10^9$ TEP (Tons of Petroleum Equivalent) were reported in 1988 (264.10^9 TEP in the U.S.). That represents 450 years of production that

can be compared to the 135.10^9 TEP of world remaining proven oil reserves ($3.6.10^9$ TEP in the U.S.) which represents about 40 years of production at 1987 levels (Comité Professionnel du Pétrole, 1989). And reserves are only a small part of the world resources that may, in the future, become economically or technically recoverable.

Coal is not used only as an energy source. The gases produced when coal is pyrolyzed with steam and air form a natural gas substitute with medium caloric content. When the methane is removed, 'synthesis gas' (Grainger and J., 1981) is obtained and various hydrocarbons may be synthesized from it by reaction between carbon monoxide and hydrogen. Liquids are also produced during coal pyrolysis. These liquids have been used as fuel and they may also provide the initial feedstock for the organic chemicals industry. Carbon itself, in various forms, is an important industrial material. For example, active carbons can be made from coal. Having fine pores and extremely large surface area, these carbons are used as adsorbents.

Potential uses of coal are diverse and important. Better knowledge and control of the mechanisms of these different reactions are thus needed to optimize the use of coal, decrease the costs, improve pollution control (especially production of sulfur dioxide, nitrogen oxides and carbon dioxide) and discover new possibilities.

1.2 PHYSICAL PROPERTIES OF COAL

Formation of coal started million years ago from partially decomposed plant debris. Once plant debris has accumulated under appropriate conditions, the formation of peat gradually occurs. Peat is the name given to the material formed during the initial stages of this process. To become coal, peat must progress through what is called "coalification" process. This process is characterized by changes in the constituent of the debris such as an increase in the carbon content, alteration of the functional groups, etc. under heat and pressure developed because of the overlying sedimentary cover (Bouska, 1981).

The extent of this metamorphosis determines the rank of coal. In practice, the rank of a coal is assigned according to its fixed carbon value or its heating value. Coals of different ranks have been given different names from lignite (low carbon content) to anthracite (high carbon content). The fixed carbon value is the weight percentage of carbon in the coal after subtraction of moisture, ash and volatile matter (three components that are also very important to describe a coal). Ash is the residue that remains after combustion of a coal sample, and volatile matter is the material (all the gases, other than water vapor) driven off by heating a coal sample in the absence of air. Usual carbon values for the different classes of coal are: 70 for lignites, 75 for subbituminous, 85 for bituminous and 94 for anthracite (Speight, 1983). A second important characteristic of a coal (because of ecological and environmental considerations) is its grade, that refers to the amount and the kind of inorganic material bound into the coal. Among a variety of inorganic components (N, Cl, F, S and others),

sulfur is perhaps the most significant because it is converted to gaseous sulfur dioxide, a toxic and corrosive pollutant, when coal is burned.

In addition to differences in elemental composition, coals are generally characterized by macroscopic heterogeneity. When examined under a microscope, coal turns out to be a complex mixture of physical constituents called **macerals**. These entities that are optically differentiated by their general appearance (shape and structure) as well as by their color and reflectance, can be classified into three groups: vitrinite, exinite and inertinite (Stack, Mackowsky et al., 1975). These three types of macerals have different properties and we will see later the importance of the maceral constitution of a coal on the mechanisms that are involved in its use.

Porosity is among the most important physical characteristics of coal because it influences the reaction of coal with various reactants. Porosity is expressed as the percentage of void volume per volume of coal. Experimental data show that porosity ranges from 25-30% in subbituminous coals to as low as 1-3% in bituminous coals (87-89% carbon) before increasing again among anthracites (Berkowitz, 1985).

According to the IUPAC classification (IUPAC, 1972), pores in coals and chars can be distinguished into:

- macropores (pores with diameters $> 500 \text{ \AA}$),
- mesopores (pores with diameters in the range $20\text{-}500 \text{ \AA}$),
- micropores (pores with diameters between 8 and 20 \AA), and
- submicropores (pores with diameters smaller than 8 \AA).

To these pore classes we should add the large macropores as the class of macropores having diameters larger than 1 mm. These pores are easily detected with optical microscopy methods.

1.3 COAL PYROLYSIS

Coal pyrolysis is the first stage of all direct coal utilization processes. During this stage, coal is heated in inert (N₂) or reactive (O₂/N₂ mixtures) atmosphere and undergoes chemical transformations releasing volatiles (with high hydrogen content) and leaving a solid residue very rich in carbon. Some coals, called plastic coals, soften and become plastic during a limited range of temperature.

The complex morphological transformations occurring during pyrolysis transform coal into a porous solid called "char" or "coke" that is burnt in the subsequent gasification or combustion stage.

1.3.1 Devolatilization

When coal is heated, it releases gas and condensable vapors. By heating at a slow and uniform rate, it is possible to distinguish three more or less distinct regimes. First, at low temperature (under 350 °C) relatively small quantities of many species are released (essentially loosely bound H₂O and CO₂). Above the temperature called temperature of decomposition that is about 350 °C (Berkowitz, 1985), primary devolatilization occurs, with a mix of molecules, from low molecular

weight gases and chemically complex liquids and semi-solid tars as the product (Grimes, 1982). This primary devolatilization is essentially complete at 550 °C. In the range 600°C-800°C, a secondary degasification takes place, producing H₂ and CH₄ as the major products (Berkowitz, 1985).

Devolatilization has been studied using different experimental methods. Thermogravimetric measurements give the rate of the decomposition reaction, continuously measuring the weight of a heated coal sample in a microbalance (Howard, 1963). This method gives mainly information on the total weight loss. To determine the release rate of each of the volatile gases, thermovolumetric measurements are required. These are done by heating a coal sample at a constant rate and frequently analyzing the released gases, using either gas chromatography for slow rates or mass spectrometry for fast ones (Judkins, Fulkerson et al., 1991).

Van Krevelen (van Krevelen, 1961) and Berkowitz (Berkowitz, 1985) summarized the influence of different parameters on this devolatilization.

- Increasing rank increases the temperature at which primary devolatilization occurs, and decreases the maximum rate of loss (this is expected since increasing carbon content corresponds to less potential volatile matter).
- From the petrographic point of view, exinite shows the largest loss of weight, inertinite the smallest.
- When the heating rate is increased, primary decomposition tends to proceed over progressively higher temperature intervals and maximum weight loss gradually increases.

- The size and porosity of coal can influence the weight loss because of the retention of volatile matter in the pore space.

1.3.2 Plasticity

The second phenomenon that occurs during pyrolysis is plasticity and it has a great influence on the physical properties of char. Some coals, referred to as caking or plastic coals, pass, when heated, through a transient plastic stage where they behave like a highly non-newtonian fluid before resolidifying. Thus, another way to classify a coal is according to whether it becomes plastic when heated.

Lignites are generally classified as non-plastic. On the other hand, bituminous coals are examples of plastic coals. As we will see later, there is no clear dividing line between these two groups and plastic coals do not appear to possess unique chemical characteristics.

The temperature range during which softening occurs roughly coincides with thermal decomposition. Bubbles of volatile gases formed during devolatilization grow inside this fluid particle of coal. The growing bubbles coalesce, the particle swells and when the walls of the particle become too thin, openings are created and the volatile matter escape. This bubbling continues until resolidification. The presence of gas bubbles at this time creates the macropore structure of char. Resolidified chars particles have many large cavities (with diameters up to several hundred microns for 0.5 to 1.0 mm particles) interconnected with smaller neck pores (Bond and Maggs, 1949; Rouzaud and Oberlin, 1990; Sinnatt, McCulloch et al., 1927; Street, Weight et al., 1968; Zygourakis, 1993) In

addition, these chars have an extensive network of micropores and submicropores (Ballal and Zygourakis, 1987).

Plasticity can become a problem when coal particles agglomerate reducing, for example, the permeability of the fluidized bed used in the production of synthesis gas from coal (Forney, Kenny et al., 1964).

The first characterization of the plasticity of a coal is its free swelling index. This is obtained by a standard test (Hessley and Reasoner, 1986), during which a finely powdered coal is heated at a fixed heating rate in a crucible. This test is essentially made to determine if a coal is fusible, and the ratio of volumes (before and after the heating) gives the swelling index.

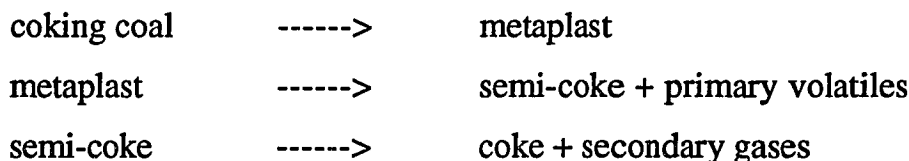
Other methods use dilatometers or plastometers. While a coal sample is heated at a constant rate, a dilatometer measures volume change by observing the vertical displacement of a counterbalanced piston that rests on the coal in a guide tube. A plastometer evaluates the apparent fluidity of the coal sample, studying the resistance offered to the rotation of a movable unit. A complete description of different types of these machines can be found in articles written by Hessley (Hessley and Reasoner, 1986), and by Loison (Loison, Peytavy et al., 1963).

The use of these methods in different studies has shown that plasticity depends upon the nature of the coal as well as upon the process conditions. First of all, inertinites do not soften at all and exinites show the most plasticity (van Krevelen, 1961). Coals showing the biggest dilatation and the largest plastic temperature range have ranks corresponding to a carbon content of 88% and 29% of volatile matter (Grimes, 1982), (van Krevelen, 1961).

The most important parameter influencing plasticity is the heating rate. With higher heating rate, fluidity and swelling are increased and plastic range is broadened. On the other hand, all coals can be devolatilized without swelling if the heating rate is sufficiently low (Dulhunty and Harrison, 1953). The same result can be obtained at very low pressure, with small enough particles or by preoxidation (Howard, 1963).

1.3.3 Physicochemical Mechanisms of Pyrolysis

The most common phenomenological theory for pyrolysis has been given by Van Krevelen (van Krevelen, 1961) distinguishing three successive reactions:



Coal is first transformed by thermal depolymerization into a fluid mass called 'metaplast'. The metaplast is then decomposed by cracking into volatile primary gases and solid semi-coke. These two reactions take place at the same time. Solid coal, fluid metaplast, primary gases escaping through metaplast and solid semi-coke, all exist simultaneously. The third reaction (secondary devolatilization) represents what is going on after the plastic range.

As Van Krevelen (van Krevelen, 1961) pointed out, this is a much too simple mechanism to provide a complete description of the complicated decomposition process. The metaplast is merely an intermediate that represents no real chemical species. This kinetic scheme was used by Oh

(Oh, Howard et al., 1984) to model the coupled effects of mass transport and chemical reactions in softened coal, accounting for plasticity and treating volatiles transport in terms of bubble growth and diffusion to the particle surface.

Since then, a more physically correct theory has been proposed. Wiser (Wiser, 1968) was the first investigator to show the similarity between pyrolysis and liquefaction. From this observation, Neavel proposed an interesting qualitative view on coal plasticity (Neavel, 1982) Using a model attributed to Given (Given, Peover et al., 1960) describing vitrinite (the major component of coal showing plastic properties) as composed of packets (micelles) of more or less aligned molecular units (lamellae), Neavel compared pyrolysis to a transient, hydrogen donor liquefaction. Low molecular weight, hydrogen rich compounds, known as bitumens serve as the initiators of plastic behavior, beginning to melt at temperature below 200 °C and solvating the coal micelles as they loosen. As temperature increases, general mobility of the micelles begins, pyrolytic bond rupture becomes significant, additional low molecular weight compounds form, and free radicals can contact donor hydrogen in thermobitumen molecules. The coal at this moment is fluid, the bubbles of volatile matter grow and the particle swells. As the temperature is increased, the formation of free radicals exceeds the capacity of the coal to cap them by hydrogen-donor reactions, the free radicals combine or attack available large molecules, semi-coke formation increases and plasticity is lost.

This model appears to explain, in a qualitative way, a large number of observation of coal plasticity (Grimes, 1982), and is very similar to the

model developed by Rouzeaud (Rouzeaud and Oberlin, 1990), based on transmission electron microscopy observation of the evolution of coal's polyaromatic Basic Structural Units during pyrolysis. However, many aspects remain unexplained and no perfect quantitative model for pyrolysis exists yet.

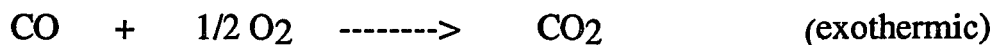
1.4 COAL COMBUSTION

Combustion is the gasification of coke with oxygen, producing heat and carbon dioxide. It is conducted in two main types of burning systems: fixed beds and fluidized beds. A complete review of the different types of combustors can be found in Coal Handbook (Rouzeaud and Oberlin, 1990). Combustion is a process comprising extremely complex reactions that involve chemical, thermal and aerodynamic phenomena, together with many coupled reactions.

Chemical reactions involving reactants, intermediates and products occur at the surface:



and in the gaseous phase:



These are only a few of the numerous reactions taking place between intermediates or products or with other elements in coke (such as N, Cl, S). A more complete description of these reactions is given by Speight (Speight, 1983).

1.4.1 Pore Surface Area and Reactivity

As we have seen before, coal is transformed to porous char (coke) during pyrolysis. The first step of combustion involves the transport (diffusion) of oxygen to the available reactive sites on the char matrix, at the particle surface and on the internal pore structure. After reacting on the surface, the gaseous products have to diffuse to the particle surface and to the bulk. This means that, due to diffusion limitations, some fraction of the internal pore surface may not be available for reaction.

As combustion takes place, carbon molecules are gasified and the pore network is modified. On one hand, new pores open up and old pores grow, increasing the surface area available to reaction. As pores continue to grow, however, neighboring pores coalesce, and the surface area decreases. Because of this transient behavior, reaction rate does not remain constant during combustion.

The rate of reaction can be written as:

$$r = \frac{dX}{dt} = \eta(T, X) A(X) S(X) f(T, C_i) \quad (1.1)$$

where X is the conversion, $S(X)$ is the internal pore surface area available, $A(X)$ is the concentration of active sites per unit surface area, $f(T, C_i)$ represents the intrinsic reaction kinetics, and $\eta(T, X)$ is the effectiveness factor accounting for diffusional limitations.

Any model describing this reaction requires knowledge the coal (rank, volatile and mineral matter contents) and an accurate characterization of the structural properties of the char (particle size, porosity and pore surface area). Since the pore structure changes drastically during pyrolysis, it is easy to understand that pyrolysis conditions are among the most important factors influencing combustion.

1.4.2 Environmental considerations

Pollution created through the use of coal as an energy source is an old problem. During the 16th century, coal was not allowed to be burned in London whenever the parliament was in session, because of sulfurous fumes and soot emission. With the current increase of public awareness about the environment and the tough clean air laws passed by industrialized nations, the only way for coal technology to survive is to improve pollutant control. Substitution of coal by natural gas is an option proposed by authors to fight against global warming (Judkins, Fulkerson et al., 1991).

The three major types of pollutants emitted by a coal-fired power plant are carbon dioxide (CO_2), sulfur dioxide (SO_2) and nitrogen oxides (NO_x). Carbon dioxide is one of the gases causing the possible global warming (often called 'greenhouse effect'). Sulfur dioxide reacting with oxygen and water in the atmosphere yields sulfuric acid that is creating acid rains. Nitrogen oxides have been identified as major factors of smog formation. Pollutant abatement technologies already exist (Berkowitz, 1979)], but with the introduction of the Clean Coal Technologies Program

(Lowell Miller, 1990) more research is needed to understand and control coal combustion.

1.5 OBJECTIVES OF OUR STUDY

1.5.1 Effect of Pyrolysis Conditions on the Macropore Structure of Chars

Previous experimental studies have shown that the pyrolysis conditions strongly affect char reactivity during combustion. Some recent results obtained in our laboratory (Matzakos, 1991) provide the main motivation for the present study

Matzakos carried out char combustion in a TGA/VMI reactor (thermogravimetric reactor with in situ video microscopy imaging) in an atmosphere composed of 33% oxygen. This reactor allows us to follow the weight of a sample and by a simple transformation the reaction rate. A video microscopy imaging apparatus was used to observe the particles and visually confirm the ignition phenomena.

Two different combustions conditions were studied. In the first one, combustion was carried out at low temperatures (400 °C to 450 °C) where char reacts in the kinetic control regime. In the second case, higher temperatures were used (550 °C to 600 °C) and combustion took place in the diffusion control regime. As is well-known (Mahajan, 1982), most of the internal surface area of coal or char particles is furnished by the numerous micropores and the micropore surface is controlling the reaction

rate when we are in the kinetic control regime. In the case of strong diffusional limitations, the utilization of micropores falls to very small levels. In chars produced from plastic coals, reaction occurs mostly at the mouths of the micropores where they open into the large macropores. Under such conditions, the small pores make a constant contribution to the reaction rate (Gavalas, 1980) and the reaction rate is controlled by the surface area of the large macropores.

Thermal ignition is an important phenomenon occurring during combustion, and that was observed with our experimental setup (Matzakos, 1991). This transient phenomenon appears when the rate of heat convection is not fast enough to dissipate the heat released by the exothermic reaction occurring in the char particle. The particle reaches an ignited state characterized by a luminous flame and there is a sharp increase of the reaction rate.

The ignition temperature is the temperature at which this phenomenon starts, and different studies have linked its value to the physical characteristics of the particles. Models and experimental studies showed that ignition temperature is lower for larger particles (Chen, Fan et al., 1984) and when larger macropores decrease diffusional limitations (Sotirchos and Amundson, 1984). An external temperature gradient is also a cause for ignition, and this gradient can be induced by a less efficient heat removal due to lower effective thermal conductivity that is directly linked to higher porosity.

These observations provide the motivation for our study. All coal utilization processes carry out combustion at high temperatures where intraparticle diffusional limitations are important. In the diffusion control

regime, the large macropores control the reactivity and particles produced under different pyrolysis conditions show different reactivity and ignition behavior. Finally, pyrolysis conditions seem to influence the macropore structure of plastic coal particles. Thus, a systematic study of the macropore structure of char particles produced in different pyrolysis conditions is necessary (Zygourakis and Sandmann, 1988) to

- analyze and explain experimental results on char reactivity during combustion,
- elucidate the fundamental mechanisms of char combustion, and
- obtain accurate measurements of the physical structure parameters required to develop predictive combustion models.

In this study, we will investigate the influence of the following pyrolysis conditions on the macropore structure of produced chars.

(A) The rate at which the particles are heated.

(B) The final heat treatment temperature.

(C) The composition of the atmosphere in the reactor.

These three parameters influence significantly the char reactivity during combustion (Matzakos, 1991).

1.5.2 Development of Experimental Techniques for Macropore Structure Analysis

To completely characterize the macropore structure of char particles, it is necessary to measure the following structural parameters.

- The average size particle.
- The average macroporosity.
- The average macropore surface area.
- The pore size distribution.

Many methods trying to describe the internal structure of a solid exist. All of them have limitations and the assumptions they are using should be made very clear before any interpretation of the results. A brief review of the most commonly used methods for pore structure characterization follows.

Heat of wetting -- A weighed sample of coal is immersed in a known volume of a suitable liquid (usually methanol). The internal surface can be calculated from the calorimetric measurement of the heat released, assuming there is no chemical interaction between the coal and the wetting liquid (Bond and Maggs, 1949). But, some authors have shown the existence of such interactions (Nelson, Mahajan et al., 1980).

Adsorption of gas or vapor -- This technique measures the volume of gas (H_2O , N_2 , O_2 , CO_2 , CH_4 , Xe , CH_3OH and others) sorbed at monolayer capacity and uses the slope of the isotherm to calculate surface

area and pore size distribution. Very different results have been found for the same coal or char, depending on which adsorbate is used (Mahajan, 1982). The other major limitation of these methods is that they can only characterize very small pores (in the size range of the gas molecules).

Mercury porosimetry -- Pore size distribution and porosity of coal can be determined by measuring the volume of mercury forced into coal as a function of applied pressure. Pore radius corresponding to pressure P is calculated from a very simple equation (Mahajan, 1982). However, narrow openings or constrictions between larger pores complicate the analysis. This creates problems for the study of chars produced by pyrolysis of plastic coals since many of their big size pores are accessible only through tight necks (if they are accessible from the outside).

Small angle X-ray scattering -- X-rays are formed into a well-defined beam that strikes the coal sample. Although most of the X-rays are either absorbed or pass through the sample without being affected, a small fraction of the radiation is emitted in directions other than that of the incoming beam. The information about the structure of the sample is obtained by analyzing measurements of the scattered intensity at a series of scattering angles. This method (Durif, 1963) avoids chemical interaction with the sample and is not limited to pores open to the exterior. But, it is not easy to use and is not commonly used for char pore characterization.

Due to the serious limitations of all the previous methods, we have decided to use a digital method based on video microscopy and image processing for macropore structure analysis. For years, microscopic

investigations have been used to study pore formation during pyrolysis of coal (Mackowsky and Wolf, 1965) but these studies were purely qualitative. Improvements in the quality of digital image processing and analysis programs allow accurate determination of statistical estimates for pore structure parameters from the study of 2D cross section images of char (Zygourakis, 1993). These data can also be used in a stereological method to obtain, assuming many geometric factors, a 3D pore size distribution (Glass, 1987). This direct method was chosen for this study to obtain all the information needed to describe char particles.

We have improved the analytical technique previously developed in our laboratory (Glass, 1987) for accurate characterization of the macropore structure of pyrolyzed coal particles. This technique was then systematically applied on particles produced at the different set of pyrolysis parameters and the results obtained were used to explain the observed experimental trends in char reactivity during combustion

CHAPTER 2 EXPERIMENTAL EQUIPMENT AND PROCEDURES

2.1 PYROLYSIS

2.1.1 Choice of coal

The coal we chose comes from the Argonne premium coal sample program (Vorres, 1990). This program is intended to provide eight coals of the highest quality for basic research. All samples of each of these coals are stored under nitrogen atmosphere in small sealed ampoules. These samples are chemically and physically as identical as possible and have well-characterized chemical and physical properties. The use of a coal from this program makes possible to compare one group's results to results obtained by other research teams using the same coal.

Since the macropore structure of non-plastic coals does not change significantly during pyrolysis (Glass, 1987), we studied a plastic coal from the Argonne Laboratory program referred to as Illinois #6 with a free swelling index of 2.13. It is a high volatile bituminous with a fixed carbon value of 40.9% mmf and 36.9% of volatile matters. It is very rich in

vitrinite (85%) with 10% of inertinite and 5% of liptinite (all are on a mineral matter free basis) (Vorres, 1990).

2.1.2 Particle size

If one uses very small particles, a maceral segregation problem can appear due to the different hardness of the various macerals. Since different macerals display different plastic properties, it may be difficult to draw general conclusions from studying small particles (Hamilton, 1980). With bigger particles, on the other hand, intraparticle temperature gradients may appear at high heating rates leading to uneven devolatilization patterns inside the coal particles.

To avoid maceral segregation problems, we chose to use particles in the 500-595 μ m size range (mesh 28-32). Earlier studies (Glass and Zygourakis, 1988) have shown that particles of this size do not have significant intraparticle gradients in our pyrolysis reactor. Samples in the desired size range were obtained by sieving the coal particles contained in the nitrogen-atmosphere ampoules received from the Argonne Coal program. All samples were stored in a vacuum desiccator.

2.1.3 Pyrolysis Reactor

Different types of reactors have been used to perform laboratory pyrolysis experiments. Often, captive sample reactors (Hamilton, 1980) are used for pyrolysis experiments. Other reactors, approximating more closely actual operating conditions, can operate with a continuous feed

system. These are fluidized bed reactors (Birch, Hall et al., 1960), entrained flow reactors (Moseley and Paterson, 1965) and free-fall reactors (Street, Weight et al., 1968). Captive sample reactors have many advantages: heating rates are very well defined, their design is simple, it is really easy to collect samples at intermediate conditions and, with the help of attached video equipment, individual particles can be continuously observed during a run.

For this study, a captive sample reactor was used (Figure 2.1) with the shape of a cylinder measuring 3 inches in diameter and 2 inches in height (Glass and Zygourakis, 1988). A water cooled jacket is used to maintain the large thermal mass of the reactor at a constant temperature. The top of the reactor is a quartz viewing window, allowing the pyrolysis to be viewed directly with a microscope and taped on a S-VHS videotape recorder (Panasonic, AG7300) through a color video camera (Javelin, Chromachip II) with 760x485 lines resolution.

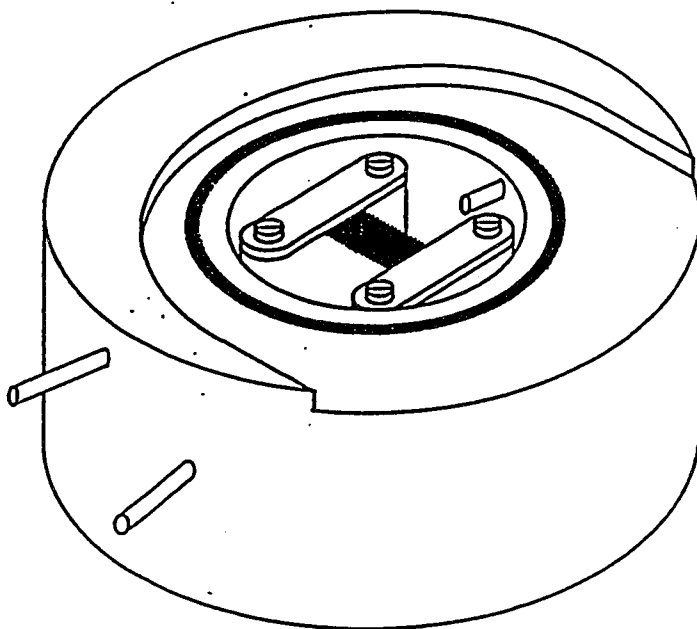


Figure 2.1: Pyrolysis hot-stage reactor

The reactor has gas inlet and outlet ports at the top and the gas flows directly over the platinum pan containing the sample. This flow sweeps away the volatiles escaping from the particles during pyrolysis, keeping the quartz window free of condensable that would obscure the view. The flow of nitrogen and oxygen to the reactor is controlled by two mass flow

controllers (MKS, 1259B). The platinum pan is electrically heated through two high amperage electrodes and a heating element covered by ceramic to evenly distribute the temperature. Temperature is measured with an chromel-alumel thermocouple (Omega, K) placed so that it touches the platinum pan. The chosen size of the particles allows us to assume that the particle temperature is uniform and equal to the temperature of the pan.

The reactor is controlled by a microcomputer (Digital Equipment Corp, PDP 11/23+) that adjusts the gas flow rates, controls the reactor temperature and performs the data acquisition tasks (Figure 2.2). A complete description of the heater control, the remotely activated mass flow controllers and the overall computer control can be found elsewhere (Matzakos, 1991). The temperature controller performs well for our pyrolysis conditions. Steady state temperatures are very stable (the error is at most 0.2 °C at steady state conditions) and the heating rates ramps are very linear. The L1 norm of the temperature error is of the order of 1 °C for rates of 0.1 and 1 °C/s, and at the order of 1 °C for rate of 10 °C/s, with slightly larger errors at the corners of the ramp for a few seconds (Matzakos, 1991).

2.1.4 Typical pyrolysis experiment

A typical experiment includes the following stages:

1. Eight particles of the 28-32 mesh range are removed from the vacuum desiccator and are immediately placed in the pan, in a configuration that keeps them away from each other to prevent agglomeration during the plastic phase.

Figure 2.2: Schematic showing the video microscopy system for the hot-stage reactor

2. The sample in the reactor is held at 150 °C in nitrogen (or 5% oxygen/95% nitrogen) flow for a few minutes to remove any moisture present. Then it is ramped to 200 °C which is the starting point of pyrolysis.
3. The pyrolysis ramp starts and the temperature is increased at a constant rate (0.1 °C/s, 1 °C/s or 10 °C/s) until the final heat treatment temperature or HTT (500 °C or 700 °C) is reached. The temperature is held constant at HTT for a soak time of 3 minutes. The reactor is then cooled rapidly to room temperature.
4. The char particles are collected and stored. Particles from several runs at the same pyrolysis conditions are used to prepare polished sections for macropore structure analysis.

2.2 Particle swelling during pyrolysis

The swelling of the particles, at different conditions of pyrolysis, has been observed qualitatively through the optical microscope and video camera attached to our reactor. Quantitative statistical data have been obtained by studying the projected area of the particles produced under different pyrolysis conditions.

After the end of pyrolysis, the char particles were placed on a glass dish and observed under transmitted light on an inverted optical microscope (Jena, Sedival) using a video camera (Javelin, Chromachip II). Digital images of the particles with 640x480 pixel resolution were acquired using a frame grabber (Imaging Technology Inc., FG100) attached to the

backplane of a computer (Digital Equipment Corp., VAXstation II/GPX). These digital greyscale images (256 levels of greys) were then analyzed using an image analysis software package (RHR Software, Icometrics). The analysis procedure consisted of the following steps.

1. **Contrast Enhancement:** All digital images were stretched to increase the contrast between bright and dark areas.
2. **Segmentation:** The pixels of relative intensity smaller than 0.4 (where 0.0 is black and 1.0 is white) were selected to create a binary image representing the coal matrix.
3. **Smoothing:** One dilation and one erosion were applied to the binary image to smooth its edges.
4. **Analysis:** The binary images were analyzed to obtain the following measurements of the projections of char particles: (a) total projected area, (b) perimeter of particle projection, (c) longest chord of particle projection and (d) shortest chord of particle projection. From these primary measurements, other important properties of the char particles such as area-equivalent radius and elongation were computed.

The size of the sample necessary to obtain measurements of a property x with error smaller than a specified limit was estimated by the method detailed by Hildebrand (Hildebrand, 1986). A small sample of n particles was first used. From the data of this sample, an estimate of the standard deviation s^2 was obtained as:

$$s^2 = \frac{\sum (x_i - \mu)^2}{n - 1}$$

where μ is the sample average of the measured property x . The size N of the total sample needed to have an error smaller than d with a confidence of α is given by the formula:

$$N = \frac{t_{1-\frac{\alpha}{2}}^2 s^2}{d^2}$$

where $t_{1-\alpha/2}$ is obtained from the Student t-distribution table (Hildebrand, 1986). and is function of the degrees of freedom n . Everything has to be checked with the estimates of the mean and of the standard deviation from the final sample.

2.3 Macropore structure analysis

The key steps in our method for macropore structure analysis are:

- (a) the preparation of polished cross sections of char particles,
- (b) the acquisition of digital images of the particle cross-sections using reflected light microscopy, and
- (c) the characterization of the macropores using digital image analysis.

2.3.1 Preparation of the polished cross sections

Particles from several runs at the same pyrolysis conditions were first encapsulated in a resin block. The resin that should be used for the preparation of polished sections of char particles must meet the following requirements:

- It must be translucent for a better contrast between char and resin on the images given by the reflected light microscope and the video camera.
- It must be very fluid to penetrate the pores open to the exterior.
- It must cure in a reasonable amount of time, at room temperature, without shrinking, giving a very hard polymer.

A new resin was designed with the help of the team working on polymers in the laboratory of Dr. Armeniades at the department of Chemical Engineering at Rice University. The cure starts when mixing, in weight ratio 11/30, the two components A and B described below:

Component A

- 2 moles of diethylene triamine (MW=103 g/mole))
- 1 mole of ethylene glycol dimethacrylate (MW=198 g/mole)

Component B

- 1 mole of trimethylol propane trimethylacrylate (MW = 297 g/mole)
- 5 epoxide equivalents of Shell Epon 826 (1 equiv.=180g) (Shell Chemical Company, 1990).

Particle Embedding: About forty particles are placed at the bottom of a plastic mold that has been treated with a release agent (Buehler, Release agent). A circular mesh is placed on the top of the particles so that they cannot float to the surface of the fluid resin. The resin is poured in the mold under vacuum that is maintained for about five minutes to allow

bubbles to escape (Figure 2.3). After about a week of curing, the samples are unmolded and labeled.

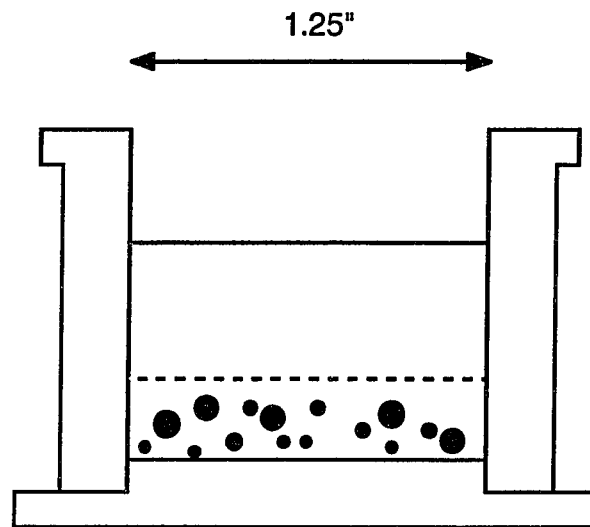


Figure 2.3: Embedding of the particles

Grinding and polishing: The samples are first beveled on a belt sander. Grinding and polishing are then performed on a polisher (Buehler, Minimet). For grinding we used grit 400 and 600 paper disks (Buehler, Carbimet disc) with water. In the polishing stage, we used alumina suspensions with particle size of $1.0\ \mu$ (Buehler, Alpha micropolish II), $0.3\ \mu$ (Buehler, Alpha micropolish II) and $0.05\ \mu$ (Buehler, Gamma micropolish II) and two different polishing cloths for $1.0\ \mu$ (Buehler, Microcloth) and for $0.3\ \mu$ and $0.05\ \mu$ (Buehler, Texmet). The settings for

the polisher speed and time used at the different stages are shown in Table 2.1.

TABLE 2.1
Steps in Grinding and Polishing Procedure
 (All settings are for the Buehler Minimet Apparatus)

Step	Abrasive or Polisher	Grit or particle size	Speed setting	Time setting
1st grinding	Buehler, Carbimet	400 grit	3	4
2nd grinding	Buehler, Carbimet	600 grit	3	3
1st polishing	Buehler, Alumina susp.	1.0 μm	6	9
2nd polishing	Buehler, Alumina susp.	0.3 μm	5	9
3rd polishing	Buehler, Alumina susp.	0.05 μm	5	9

Between steps, the sample stays at least three minutes in an ultrasonic bath (Branson, Bransonic 32) to remove any particles from of the previous step.

2.3.2 Digital image acquisition

The polished sections were viewed using reflected light and a 10X objective on an inverted microscope (Jena, Sedival) equipped with a super high pressure mercury lamp. Particle cross sections were observed with a video camera (JVC, TK107OU) attached to the microscope. The video output from the camera was fed to a frame grabber (Imaging Technology Inc., FG100) attached to the backplane of a computer (Digital Equipment Corp., VAXstation II/GPX). Digital images with a spatial resolution of 640x480 pixels (8 bits per pixel) were acquired using this frame grabber and stored on the hard disk of the computer. In these greyscale images (256 levels of grey), coal appears as white (almost all the light is reflected at its surface). Resin-filled pores and the resin surrounding the particles appear as grey since resin reflects only part of the light. Unfilled pores appear black. A representative greyscale image of a particle cross section is shown in Figure 2.4.

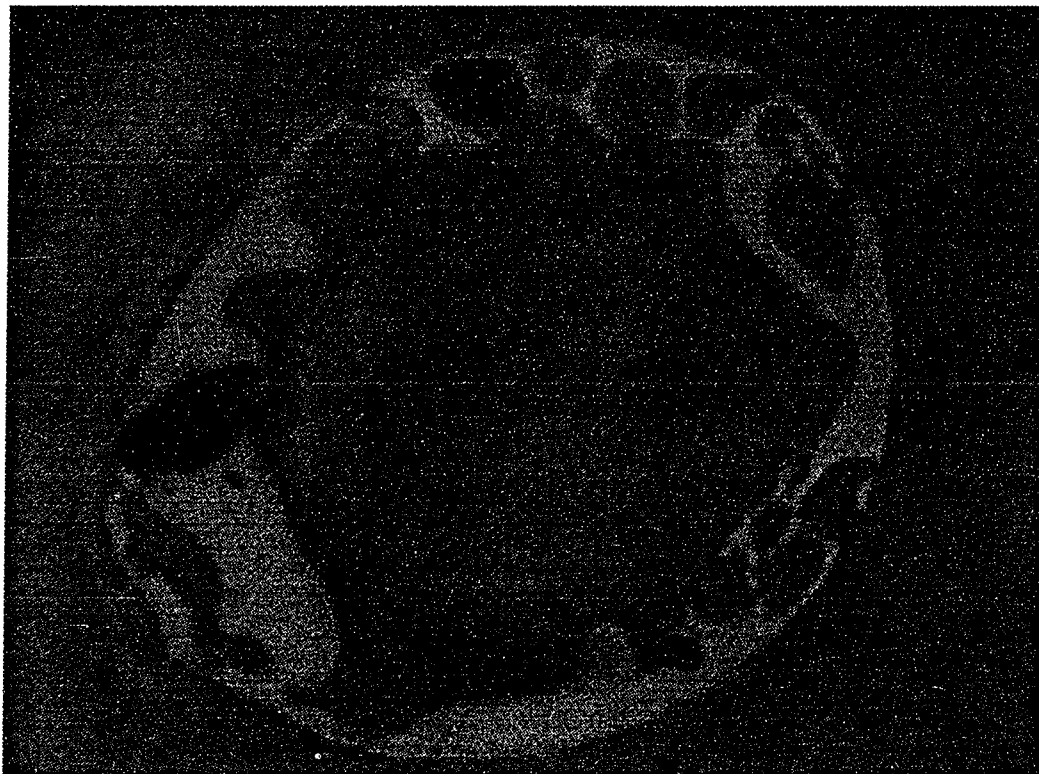
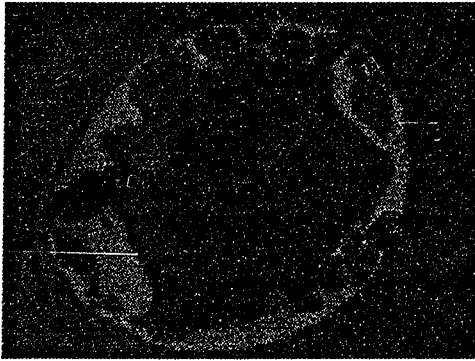


Figure 2.4: Greyscale image of a coal particle cross-section

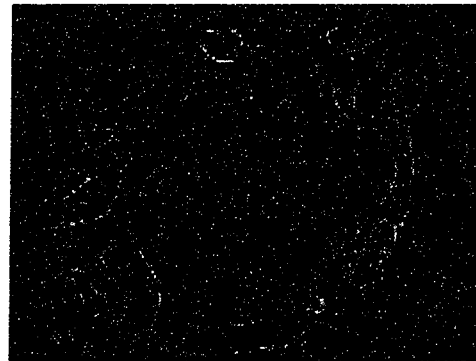
2.3.3 Image analysis

The image analysis process has been automated and consists of the following procedures:

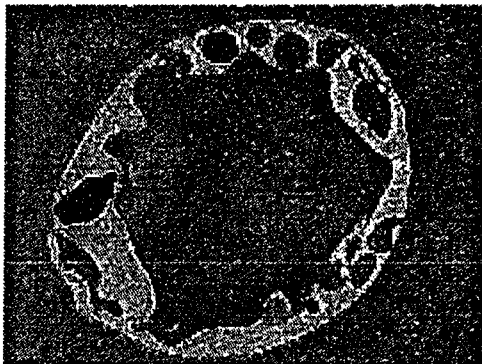
1. The greyscale image (Figure 2.5a) is first stretched to obtain a better contrast between char and resin.
2. A 3x3 gradient filter is then applied to the stretched image to delineate the edges between char and resin. The resulting image is shown in Figure 2.5b.
3. The image obtained by applying the gradient filter is added to the original image to increase the intensity of the boundaries between char and resin. The image resulting from this operation is shown in Figure 2.5c.
4. The sum image is stretched again to obtain the final greyscale image (Figure 2.5d).
5. The pixels of intensity greater than 0.4 are selected to form a binary image of the char matrix (Figure 2.6a).
6. This binary image is smoothed using a dilation/erosion process to obtain the final binary image (Figure 2.6b).
7. The smoothed binary image is analyzed to identify the macropore profiles and calculate the following quantities for each profile: (a) area, (b) perimeter, (c) longest chord that can fit in each pore profile and (d) shortest chord that can fit in each pore profile. From these primary measurements, other important properties of the pore



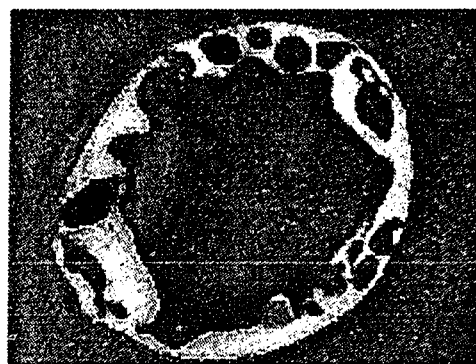
a- Greyscale image



b- Gradient filter



c-Addition of a and b



d- Stretched version of c

Figure 2.5: Processing of the greyscale image

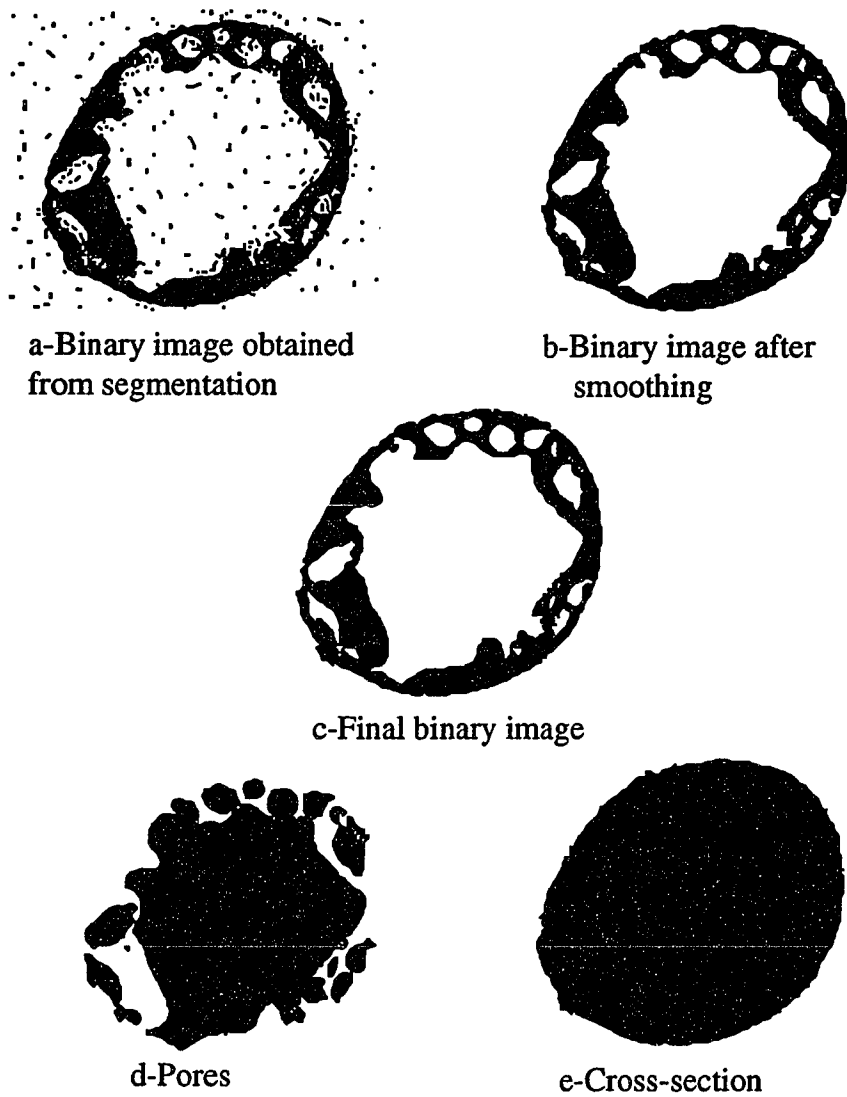


Figure 2.6: Processing of the binary image

profiles such as area-equivalent radii, elongation and shape factors can then be computed.

2.3.4 Measuring the Volume and Surface Area of Macropores

Without making any assumption on the shape of the particles and the pores, an accurate estimate of two important properties of coal can be calculated from the data on the two-dimensional pore profile: macroporosity and macropore surface area density (de Hoff, 1983).

An unbiased estimate of the macroporosity ϵ_m of coal can be obtained by :

$$\epsilon_m = \frac{A_m}{A_p} \quad (1)$$

where A_m is the total area of macropores in the two-dimensional cross sections and A_p is the total area of cross sections (char and macropore profiles).

Weibel (Weibel, 1980) also used geometrical probability theory to obtain an unbiased estimate of the macropore surface area density S_v defined as the surface area of macropores per unit volume of particle:

$$S_v = \frac{4 B_m}{\pi A_p} \quad (2)$$

where B_m is the sum of the perimeters of all macropore profiles in the two-dimensional cross sections and A_p is the total area of cross sections (char and macropore profiles). The size of the sample required to obtain

measurements with desired accuracy was estimated using the method described in Section 2.2.

2.3.5 Macropore Size Distribution

If we assume that pores are non-overlapping spheres embedded in the char matrix, a size distribution $N(r)$ of the three-dimensional pores can be computed from the size distribution of the two-dimensional pore profiles.

Consider a population of spherical pores whose radius r is randomly distributed in the interval $[0, r_m]$ and let $N(r)$ be the corresponding probability density function. Then the fraction of spheres with radii between r and $r+dr$ is given by $N(r)dr$. If this population of spherical pores is intersected with planes of random orientations, the sphere cross-sections will yield circles with randomly distributed radii. Let $n(\rho)$ be the probability density function of the circles representing the cross sections of the population of spheres intersected by a plane of random orientation. Then $n(\rho)d\rho$ is the number of circles, per unit area of intersecting plane, with radii between ρ and $\rho+d\rho$.

The relation between the two distributions $N(r)$ and $n(\rho)$ has been given by Wicksell in his study of the corpuscle problem (Wicksell, 1925), as:

$$n(\rho)d\rho = \int_{\rho}^{r_m} \frac{2N(r)\rho dr d\rho}{\sqrt{r^2 - \rho^2}} \quad (3)$$

The problem now is to unfold the three-dimensional size distribution $N(r)$ from the measurable profile distribution when no explicit analytical

form for $n(\rho)$ is available. Equation (3) must thus be solved numerically. Weibel (Weibel, 1980) reviewed the most popular methods for solving these problems. The limitations of these methods stemmed from the use of rectangular integration rules. Zygourakis and Glass (Zygourakis and Glass, 1988) improved the solution method by using trapezoidal integration rules. Then equation (3) becomes:

$$\mathbf{n} \Delta \rho = \mathbf{K} \mathbf{N}$$

Where \mathbf{n} and \mathbf{N} are the frequency column vectors for the m bins of the histogram distribution respectively in 2D and 3D and \mathbf{K} is an upper triangular $m \times m$ matrix defined by:

$$\begin{aligned} k_{ij} &= 2\Delta r^2 \left\{ \sqrt{j^2 - (i-1)^2} - \sqrt{j^2 - i^2} \right\} & \text{for } i \leq j < m \\ k_{ij} &= \Delta r^2 \left\{ \sqrt{j^2 - (i-1)^2} - \sqrt{j^2 - i^2} \right\} & \text{for } j=m \end{aligned}$$

Tests of this method on known distribution of spheres (Zygourakis and Glass, 1988) showed that (when using B-spline smoothing in least squares sense) approximately 2000 to 3000 2-D profiles are required to unfold the three-dimensional distribution within a 10% error.

We have written our own FORTRAN program to create the histogram of two-dimensional data, smooth their cumulative form (using B-spline smoothing in the least squares sense), apply the stereological method and smooth the three-dimensional data. From this distribution, values of macroporosity and macropore surface area density were calculated. One should not forget that this method makes the important assumption that the macropores are non-overlapping spheres.

CHAPTER 3

PARTICLE SWELLING DURING PYROLYSIS

3.1 SOME QUALITATIVE OBSERVATIONS

During the plastic phase, pressure builds up in the interior of the pyrolyzing particles because gas volatiles are released faster than they can escape to the outside. As a result, coal particles deform and swell during pyrolysis. These changes in the particles' shape and size have been studied qualitatively and quantitatively.

Our hot-stage pyrolysis reactor allows the use of a microscope to observe and videotape a single particle or a group of particles, during pyrolysis (Figure 2.2). The elapsed time since the beginning of the heating ramp is superimposed on each video frame. From the elapsed time and the programmed value of the heating rate we can calculate the reactor temperature corresponding to each video frame and relate it to the structural changes occurring on the video tape.

We can thus determine the temperature range over which the coal becomes plastic and releases volatiles. The approximate ranges we have observed for coal plasticity are given in Table 3.1.

Table 3.1
Temperature Ranges for Coal Plasticity

Pyrolysis Heating Rate °C/s	Lower Bound of Plasticity Range °C	Upper Bound of Plasticity Range °C
0.1	400	500
1.0	450	530
10.0	490	600

Note that at a heating rate of 10 °C/s the temperature is increasing rapidly making difficult an accurate determination of the temperature range for plasticity. At this rate, a large amount of volatiles is released in a small period of time and condensation of these gases on the quartz window is significant.

The coal plasticity ranges of Table 3.1 are in agreement with the temperature ranges where the largest weight loss or devolatilization rates were observed in a thermogravimetric reactor by Matzakos (Matzakos, 1991; Matzakos and Zygourakis, 1990) for the same Illinois #6 coal.

During the plasticity period, several gas bubbles grow and break through the surface in quick succession forcing the particles to expand and contract until they resolidify. During this stage, particles become round and an overall increase in size is observed.

The vigorousness of bubbling increases with increasing heating rate mostly because of the apparent increase in fluidity and the changing

duration of the plastic phase. At a heating rate of 0.1 °C/s, the temperature rises from 400 °C to 500°C and the volatiles are released in about 17 minutes, while at 10 °C/s the volatiles are released in about 10 seconds.

When the heat treatment temperature is 500 °C and at heating rates of 1 °C/s and 10 °C/s, bubbling has not stopped when the pyrolysis run is stopped at the HTT. Since the bubbling continues, some of the char particles are expanding while others are contracting at the end of the pyrolysis run.

In the extreme case of heat treatment temperatures of 700 °C and pyrolysis heating rates of 10 °C/s, the internal pressure buildup and the fluidity of the coal are so high that many particles collapse and become flat.

When pyrolysis occurs in the presence of 5% O₂ in nitrogen atmosphere, a very interesting change in the behavior of the particles during the plastic phase has been observed. The particles behave as if they have a less fluid external layer and gas bubbles grow much bigger before volatiles are released. At 10 °C/s for an HTT of 700 °C, we have observed eruptions of fluid matter through the surface of the particles when internal pressure is high enough to burst through the not so fluid shell. The violent release of gases makes particles "jump" from one place to another in the pan.

This behavior and the effect of preoxidation on pyrolysis (Mahajan, Komatsu et al., 1980) probably have very similar causes. The presence of oxygen leads to formation of ether-type crosslinks between the coal lamellae structure and these crosslinks decrease coal fluidity. In our case, oxygen cannot probably penetrate the entire particle causing instead loss of fluidity in a thin cell below the particle surface.

We have carried out pyrolysis experiments with low oxygen concentrations (only 5%) and short exposure times (pyrolysis at 10 °C/s or at 1 °C/s up to 500 °C) to minimize partial reaction of the coal matrix with oxygen during pyrolysis. That has been confirmed by Matzakos (Matzakos, 1991) who showed that char produced in either inert or 5% oxygen atmosphere exhibited similar devolatilization patterns and intrinsic reactivities.

3.2 PYROLYSIS CONDITIONS AND CHAR PARTICLE SIZE

We studied the size and shape of devolatilized coal particles by analyzing digital images of particles acquired after the end of pyrolysis runs. Figures 3.1 to 3.4 present representative projected profiles of particles obtained under various pyrolysis conditions.

Table 3.2 presents the effect of pyrolysis conditions on the area-equivalent radius r for the projected particle profiles computed as

$$r = \sqrt{\frac{A}{\pi}}$$

where A is the measured area of the projected particle profiles.

As stated in Section 2.2, the sample size for each set of pyrolysis conditions was chosen so as to have an absolute error smaller than 0.01 mm with a confidence of 95% for the average area-equivalent radius (radius of the circle with the same area). We should note here that the area-equivalent radius for the coal particles used for these runs was 0.349 mm. However,

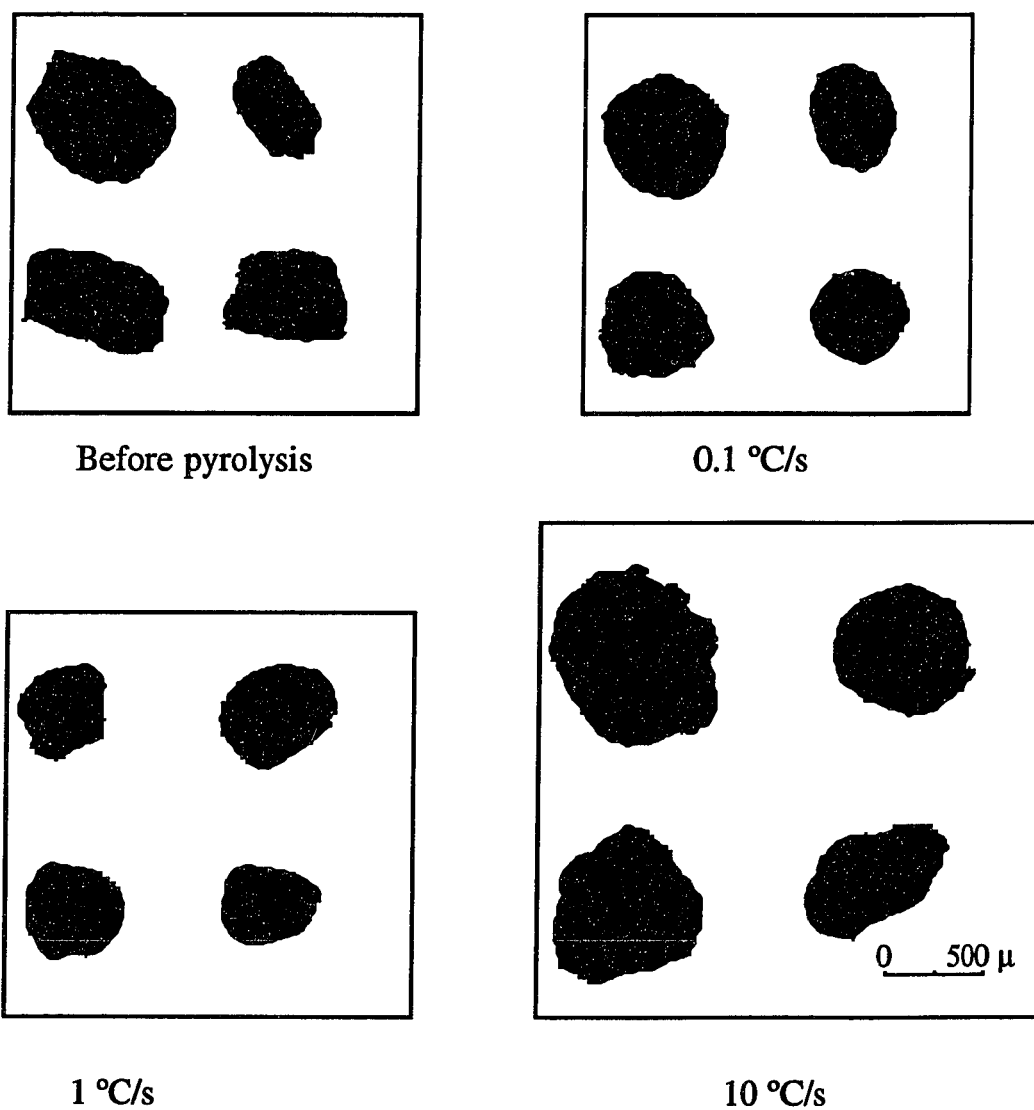


Figure 3.1: Projected areas of particles before pyrolysis and after pyrolysis at HTT 700 °C without oxygen.

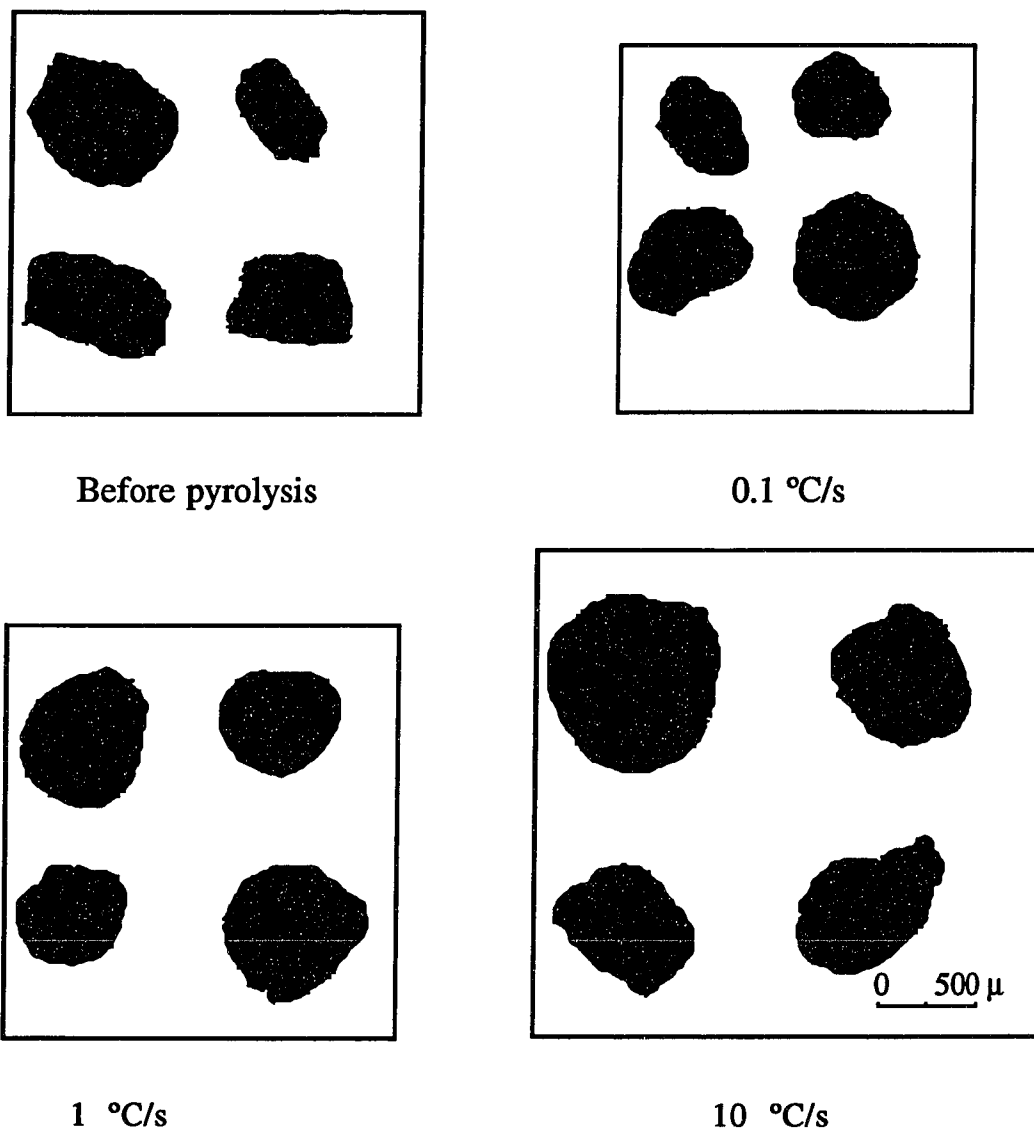
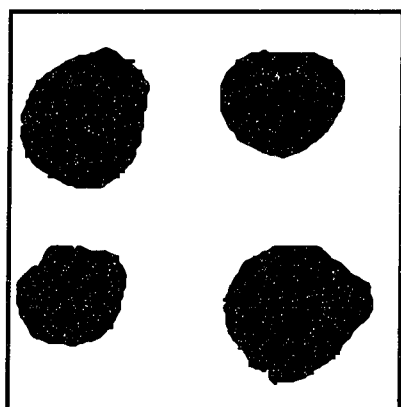
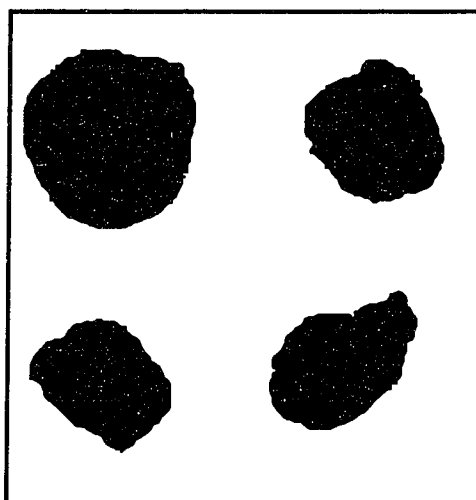


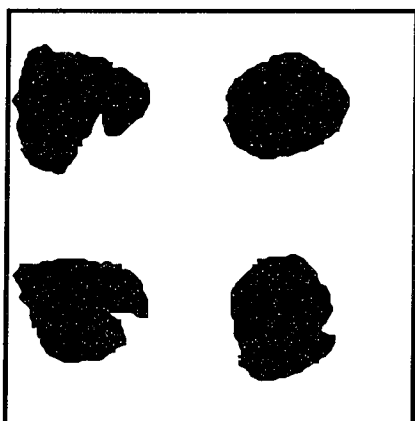
Figure 3.2: Projected areas of particles before pyrolysis and after pyrolysis at HTT 500 °C without oxygen.



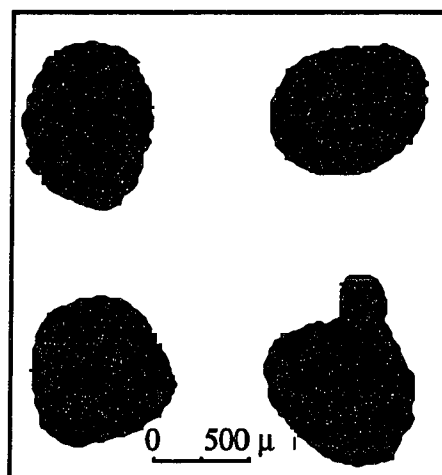
1°C/s no oxygen



10°C/s no oxygen

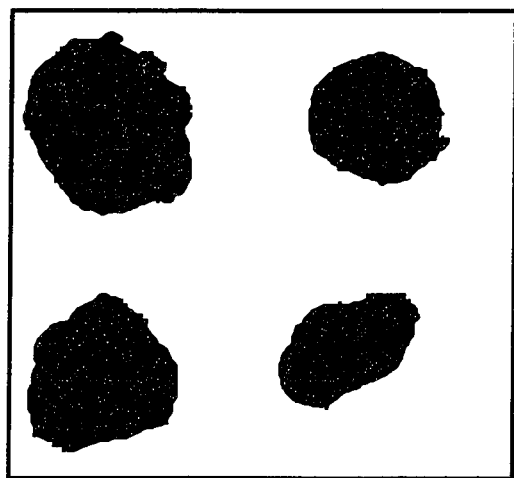


1°C/s 5% oxygen

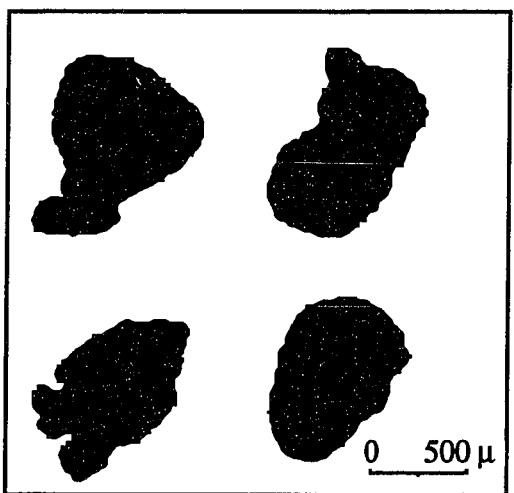


10°C/s 5% oxygen

Figure 3.3: Projected areas of particles pyrolysed at HTT of 500 °C



no oxygen



5% oxygen

Figure 3.4: Projected areas of particles pyrolysed at 10 °C/s and HTT of 700 °C

the original coal particles are not spherical having angular and elongated shapes.

Table 3.2
Effect of Pyrolysis Conditions on the Size of Char Particles

Pyrolysis Heating Rate, °C/s	O ₂ concentration %	Heat Treatment Temperature °C	Sample Size	Area- Equivalent Radius, mm
0.1	0	500	55	0.316
0.1	0	700	60	0.317
1	0	500	106	0.335
1	0	700	125	0.325
1	5	500	64	0.331
10	0	500	134	0.387
10	0	700	131	0.407
10	5	500	120	0.443
10	5	700	81	0.433

Figure 3.5 presents the effect of pyrolysis conditions on the average particle size. When the pyrolysis heating rate is low (0.1 or 10 °C/s), the heat treatment temperature and the pyrolysis atmosphere have very small effects on the average particle radius. An increase in the heating rate from 0.1 to 1.0 °C/s increases only slightly the average particle radius.

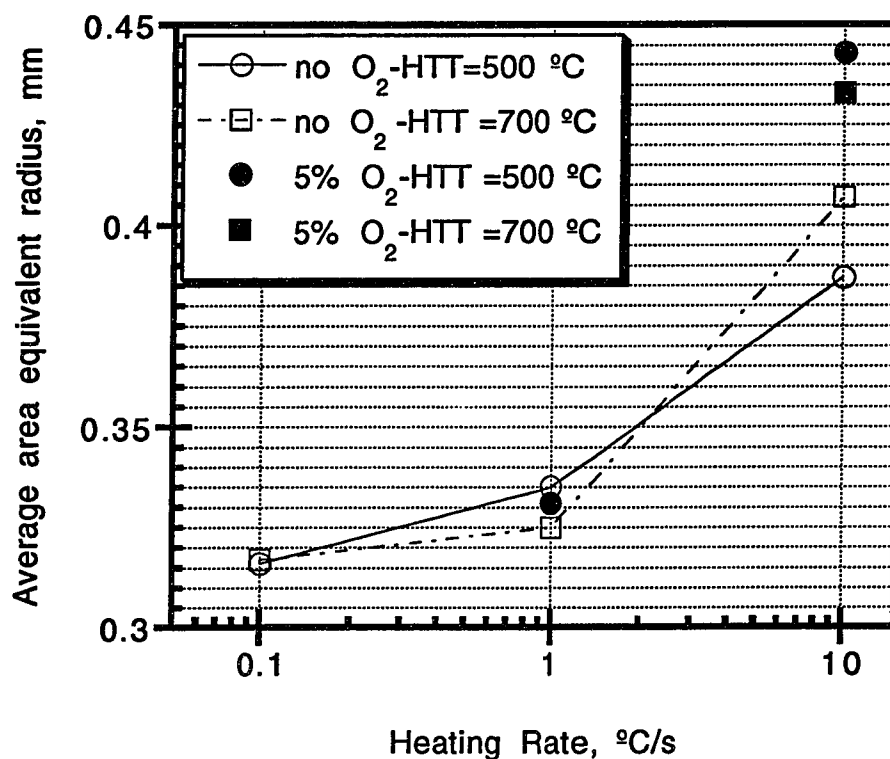


Figure 3.5: Effect of pyrolysis conditions on average particle area equivalent radius.

When the pyrolysis heating rate increases to 10 °C/s, the particles swell much more. At 10 °C/s, particles pyrolyzed to an HTT of 500 °C have a slightly smaller average particle size. This may be due to our earlier observation that some particles may be contracting at the end of the pyrolysis run (bubbling continues at this temperature). Finally, pyrolysis in a reactive atmosphere (5% O₂/95% N₂) leads to further increases in the average particle radius.

Figure 3.6 presents the effect of pyrolysis conditions on the swelling ratio calculated as

$$\text{Swelling ratio} = \left(\frac{r}{r_0} \right)^3$$

where r is the average particle radius for a given set of pyrolysis conditions and r_0 is the average particle radius for 0.1 °C/s, an HTT of 700 °C and pure nitrogen pyrolysis atmosphere.

An increase of the heating rate to 1.0 °C/s increases the swelling ratio to 1.1-1.2 for the various pyrolysis conditions in this study. At 10 °C/s heating rate, the swelling ratio increases dramatically to 1.8-2.1 for nitrogen atmosphere and 2.5-2.7 for the reactive atmosphere we tried (5% O₂/95% N₂).

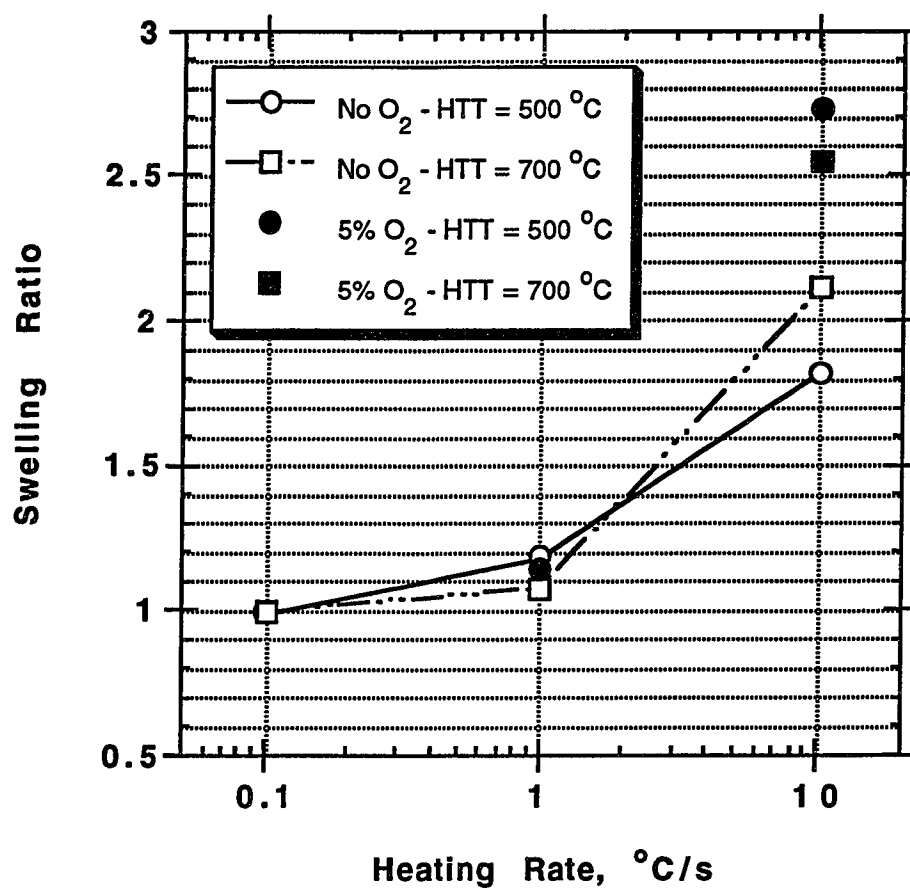


Figure 3.6: Effect of pyrolysis conditions on swelling ratio

3.3 PYROLYSIS CONDITIONS AND CHAR PARTICLE SHAPE

Coal particles in the 28-32 mesh (500-600 μm) range were used for this study. If the particles before pyrolysis were spheres, the observed

average area-equivalent radius of the particle projections would be around 0.275 mm. Our measurements gave a value of 0.349 mm (± 0.01 mm). To account for this discrepancy, we obtained the statistics on length and width of particle projections (Figure 3.7) before and after pyrolysis.

This analysis showed that coal particles before pyrolysis are more closely approximated by ellipsoids rather than spheres. Since the particles round up during pyrolysis, the char particles produced at low heating rates have smaller area-equivalent radii than the original coal particles. A comparison of Figures 3.7 and 3.8 that show particle length and width distributions both before pyrolysis and after pyrolysis at a heating rate of 0.1 °C/s (HTT 700°C, pure N₂), the decrease of elongation of the projected areas is obvious.

In the presence of oxygen, more particles are round (Figure 3.9) except at a heating rate of 10 °C/s with HTT of 700 °C where the eruptions take place (Figure 3.10). This is confirmed by the study of shape factor s defined as:

$$s = \frac{P^2}{4\pi A}$$

where P is the perimeter of a pore profile and A its area. Its value reflects the complexity of the pore boundary. It is unity if the object is a perfect circle and increases as the object differs from unity (that is the case with eruptions). In the base case (0.1 °C/s, pure N₂, 700 °C HTT) the average shape factor is 1.31 and in reactive atmosphere at

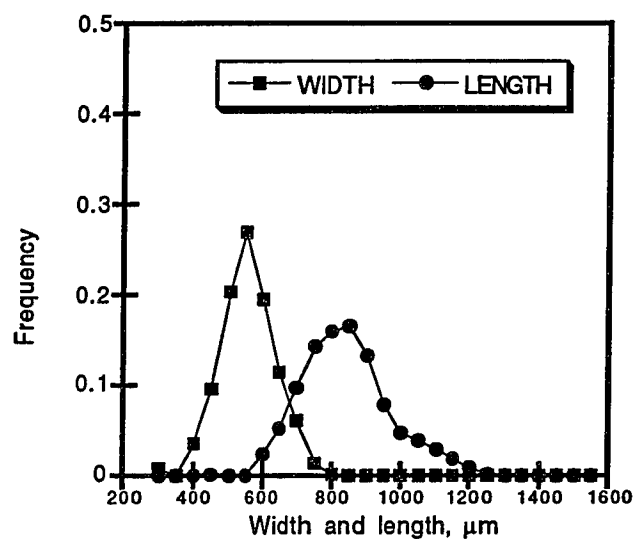


Figure 3.7: Width and length distribution of 61 particles before pyrolysis

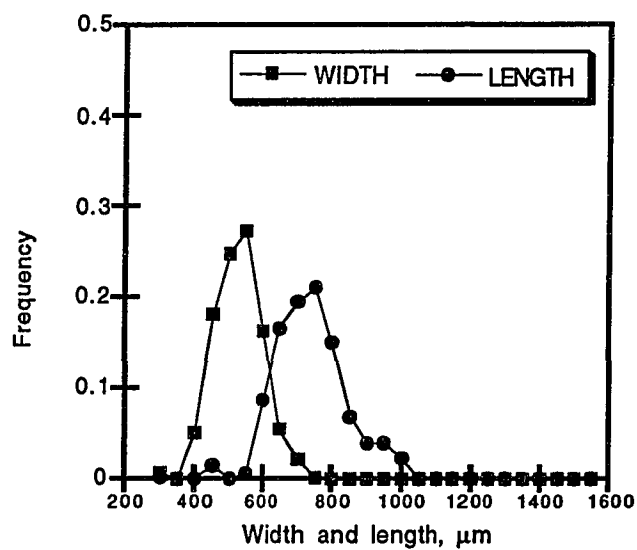


Figure 3.8: Width and length distribution of 60 particles after pyrolysis at 0.1 °C/s, HTT 700 °C without oxygen

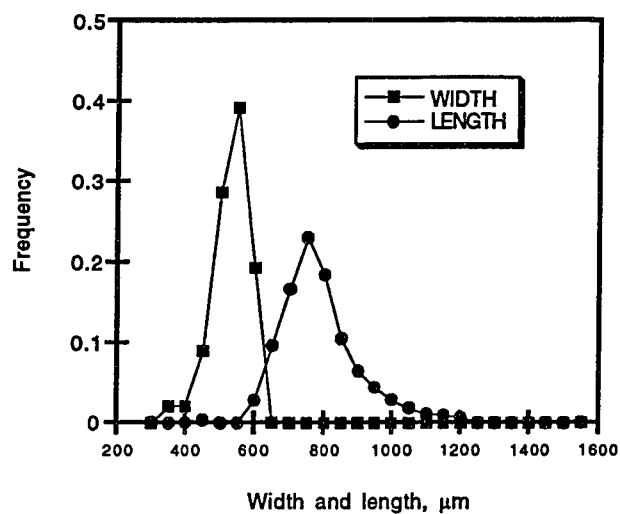


Figure 3.9: Width and length distribution of 64 particles after pyrolysis at 1 °C/s, HTT 500 with 5% oxygen

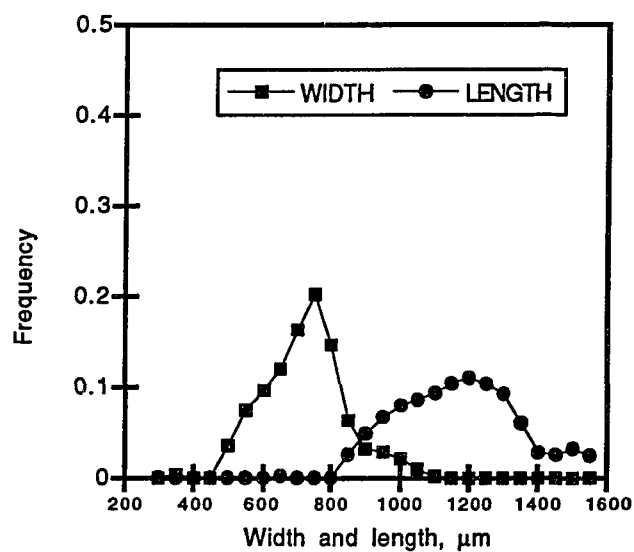


Figure 3.10: Width and length distribution of 176 particles after pyrolysis at 10 °C/s, HTT 700 °C with 5% oxygen

a heating rate of 10 °C/s with HTT of 700 °C it reaches 1.54. The distribution of shape factors for this two cases is shown on Figure 3.11. When particles have been pyrolysed at a rate of 10 °C/s with 5% O₂ in N₂ up to 700 °C, shape factors are globally higher and a large group of particles with shape factors between 2.0 and 2.1 corresponding to the particles with 'eruption bumps' (Figure 3.4).

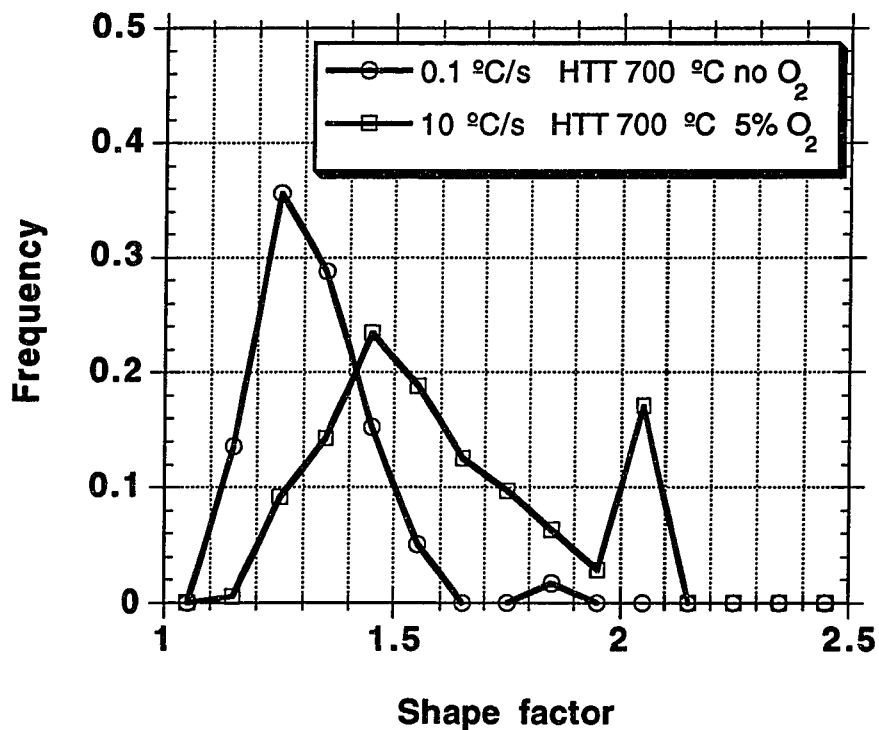


Figure 3.11: Distribution of shape factors for the base case and pyrolysis at 10 °C/s, 700 °C HTT and 5% O₂.

3.4 HEATING RATE AND PARTICLE SIZE DISTRIBUTION

The projected area size distribution of char particles does not change significantly when the pyrolysis heating rate is increased from 0.1 °C/s to 1°C/s (Figures 3.12 and 3.14). Note that for both HTT's (500 and 700 °C) the average area-equivalent radius of char particles increased only slightly when the heating rate increased from 0.1 to 1.0 °C/s.

Changes in particle size distribution are much more pronounced when the heating rate increases to 10 °C/s. As shown in Figure 3.13, the size distribution for char particles produced at an HTT of 700 °C is significantly shifted towards larger sizes. Under these pyrolysis conditions, the average area-equivalent radius of char particles is 25% larger than the base case (0.1 °C/s, pure N₂, 700 °C HTT).

The tendency for particles to collapse for heating rates of 10 °C/s and an HTT of 700 °C complicated the study of particle projected areas at these conditions. We again observe a shift in the size distribution towards larger sizes with the increasing heating rate (see Figures 3.13 and 3.15) and the average particle size is almost 15% larger than the average size observed for the base case.

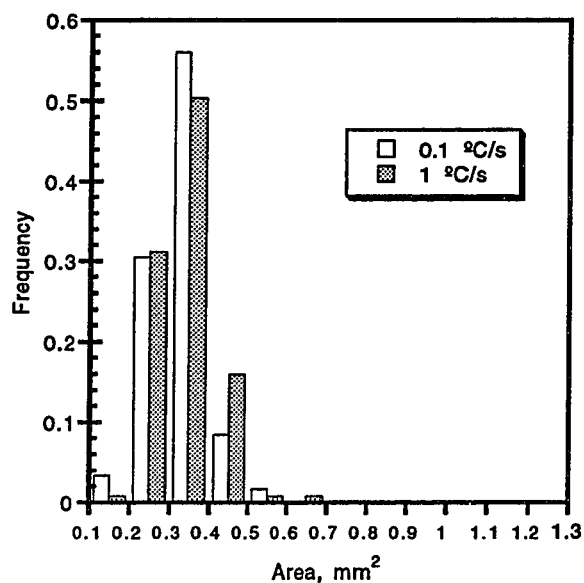


Figure 3.12: Particle size distribution after pyrolysis at HTT 700 °C, without O₂ (0.1°C/s: 60 part., 1°C/s: 125 part.)

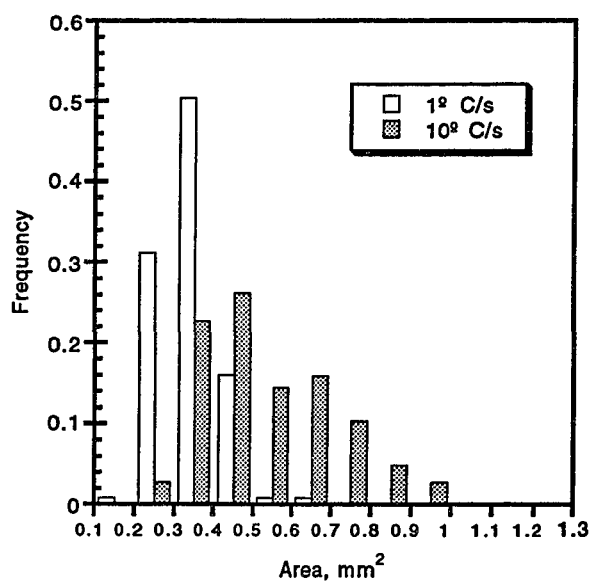


Figure 3.13: Particle size distribution after pyrolysis at HTT 700 °C without O₂ (1 °C/s: 125 part., 10 °C/s 145 part.)

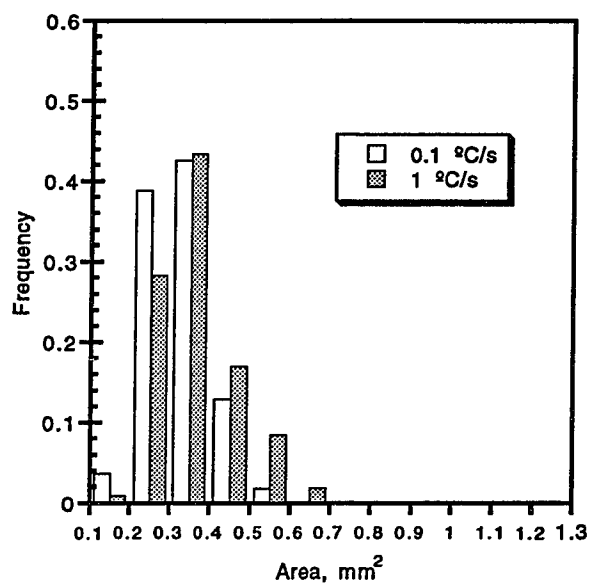


Figure 3.14: Particle size distribution after pyrolysis at HTT 500 °C without O₂ (0.1 °C/s: 54 part., 1 °C/s: 106 part.)

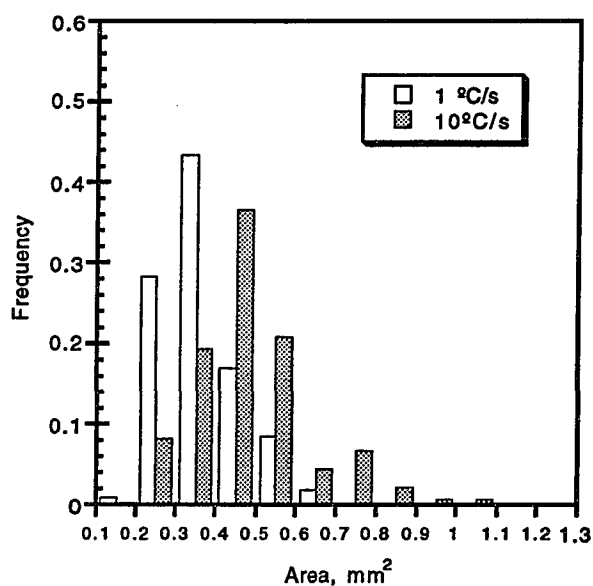


Figure 3.15: Particle size distribution after pyrolysis at HTT 500 °C without O₂ (1 °C/s: 106 part., 10 °C/s: 134 part.)

3.5 HTT AND PARTICLE SIZE DISTRIBUTION

By stopping the pyrolysis at 500 °C we do not significantly affect the statistics of particle projections for a heating rate of 0.1 °C/s. Both the average particle radius and the size distribution are similar for HTT's equal to 500 and 700 °C as shown in Figure 3.16. This can be explained by the fact that at the low heating rate of 0.1 °C/s the bubbling (and therefore the expansion and contraction) of the pyrolyzing particles has stopped when the reactor temperature reaches 500 °C. Similar results are obtained at 1.0 °C/s (Figure 3.17).

At 10 °C/s, however, particle bubbling has not stopped when the reactor temperature has reached 500 °C. At this point, some particles are expanding while others are contracting. This is why much wider size distributions are obtained for an HTT of 500 °C in both N₂ and O₂/N₂ atmospheres (see Figures 3.18 and 3.19). This phenomenon is less obvious at 10 °C/s without oxygen because of the collapsing of certain particles for HTT of 700 °C (Figure 3.19).

3.6 OXYGEN ATMOSPHERE AND PARTICLE SIZE DISTRIBUTION

Experiments with 5% O₂ / 95% N₂ mixtures were not conducted at a heating rate of 0.1 °C/s to prevent the occurrence of extensive

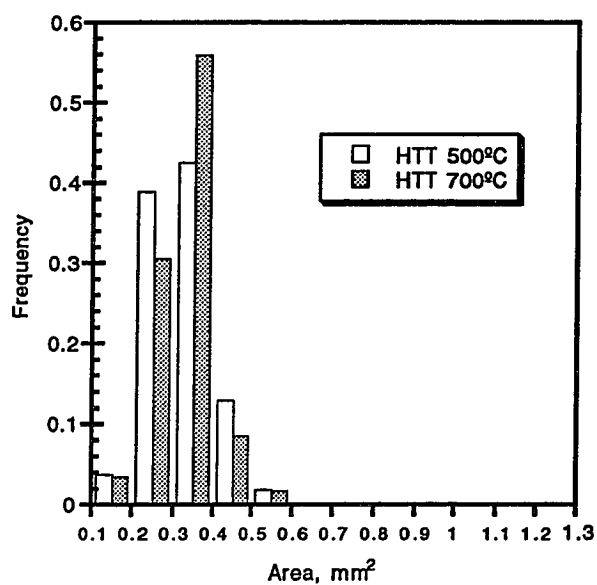


Figure 3.16: Particle size distribution after pyrolysis at 0.1 °C/s without O₂ (HTT 500°C: 54 part., HTT 700°C: 60 part.)

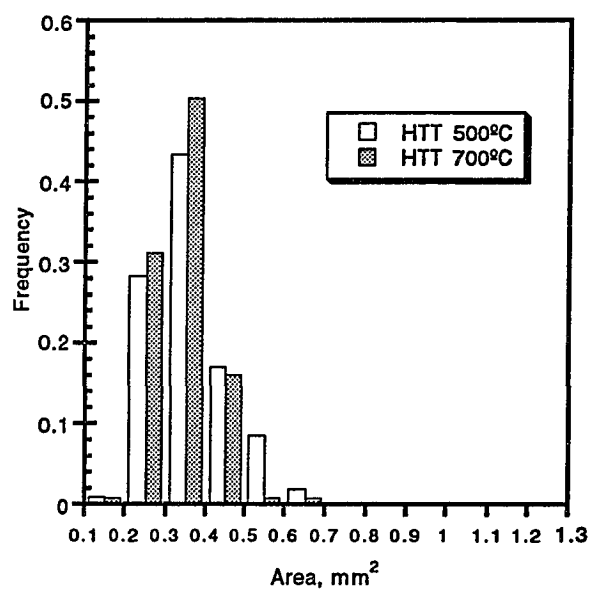


Figure 3.17: Particle size distribution after pyrolysis at 1 °C/s without O₂ (HTT 500°C: 106 part., HTT 700°C: 125 part.)

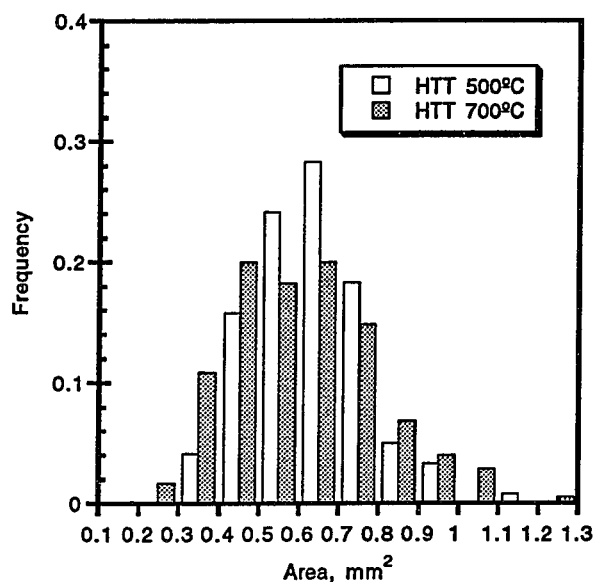


Figure 3.18: Particle size distribution after pyrolysis at 10 °C/s with 5% O₂ (HTT 500°C: 120 part., HTT 700 °C: 176 part.)

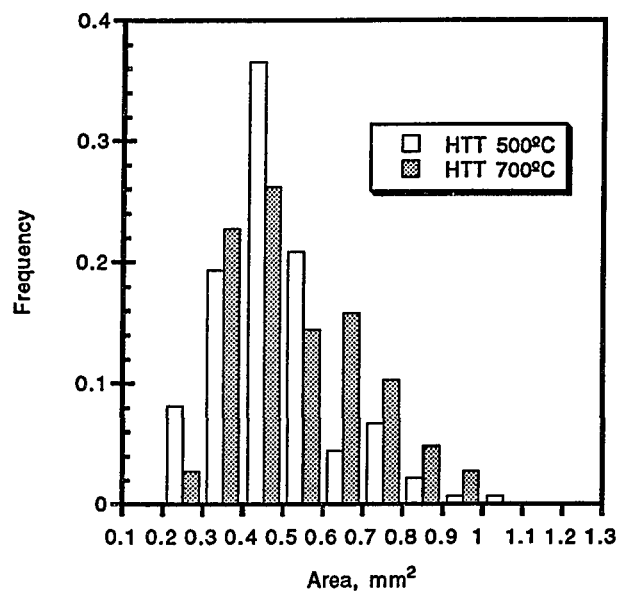


Figure 3.19: Particle size distribution after pyrolysis at 10 °C/s without O₂ (HTT 500°C: 134 part., HTT 700 °C: 145 part.)

combustion. A similar problem would be encountered at 1 °C/s and an HTT of 700 °C.

For a rate of 1 °C/s and HTT of 500 °C, the presence of O₂ does not change the average particle size (average radii are 0.331 and 0.335 mm respectively) and only slightly changes the particle size distribution (Figure 3.20).

For a rate of 10°C/s, the differences are more significant. For an HTT of 700 °C, the average particle size increases by about 7.5% and the size distribution shifts to larger sizes in the presence of oxygen (Figure 3.21). We should note, however, that the particles tend to collapse in nitrogen atmosphere, while in the presence of oxygen eruptions of internal matter are observed.

At an HTT of 500 °C (Figure 3.22), we obtained the biggest spherical particles of our study with an average particle radius of 0.443 mm, an increase of almost 14% over the average radius of the particles produced under the same conditions without O₂. The presence of oxygen enhances the effects of increasing pyrolysis heating rate on particle swelling. The size distributions of char particles produced in oxygen-containing atmospheres are wider and more shifted to the right than size distributions of particles obtained in nitrogen atmospheres and at the same high value of heating rate (compare Figures 3.15 and 3.23).

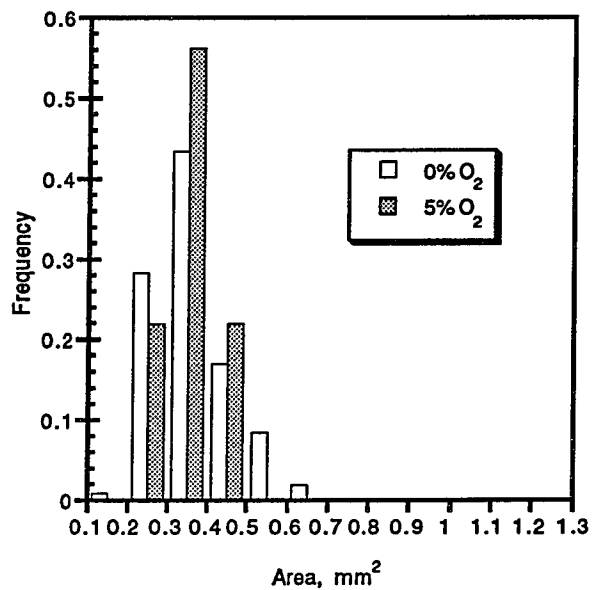


Figure 3.20: Particle size distribution after pyrolysis at 1 °C/s and HTT 500 °C (0% O₂: 106 part., 5% O₂ 64 part.)

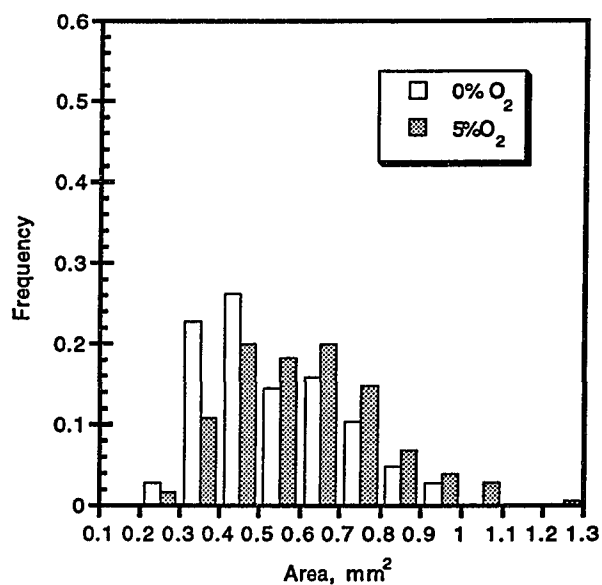


Figure 3.21: Particle size distribution after pyrolysis at 10 °C/s and HTT 700 °C (0% O₂: 145 part., 5% O₂ 176 part.)

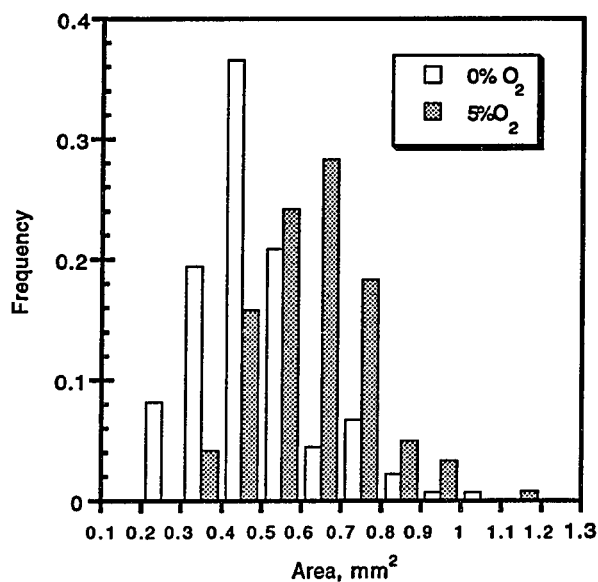


Figure 3.22: Particle size distribution after pyrolysis at 10 °C/s with HTT 500 °C (0% O₂: 134 part., 5% O₂: 120 part.)

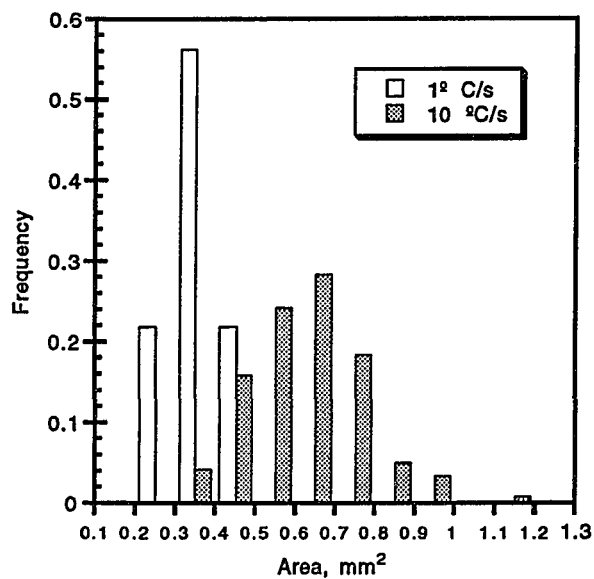


Figure 3.23: Particle size distribution after pyrolysis at HTT 500 °C with 5% O₂ (1 °C/s: 64 part., 10 °C/s: 120 part.)

CHAPTER 4 MACROPORE STRUCTURE ANALYSIS

4.1 PYROLYSIS CONDITIONS AND CHAR MACROPORE STRUCTURE

Thirty to sixty particle cross-sections for each set of pyrolysis conditions were digitized and analyzed. Figures 4.1 to 4.4. present a few representative binary images obtained from the greyscale images of particle cross-sections for the various set of pyrolysis conditions.

Note that our digital image analysis method can detect only macropores whose profiles are larger than one pixel or 1.72 mm^2 . In every polished section we prepared, only few macropores were not filled with resin presumably because they either have no connection to the outside or because their openings are too small for a resin of this viscosity to penetrate. On the greyscale images obtained from our reflected light microscope, the cross-sections of unpenetrated pores appear as black.

When the pyrolysis heating rate is increased, the qualitative changes observed in particle cross-sections involved the thinning of the macropore walls and the appearance of secondary vesicles in the walls of the biggest pores.

Char particles produced at pyrolysis heating rates of 0.1 °C/s have either one relatively large cavity or a few medium size macropores with thick walls. These samples were the only ones with significant numbers of unfilled pores. At 1 °C/s the macropore walls become thinner, but the biggest changes comes when the heating rate is increased to 10 °C/s. Particles produced at this heating rate often have one or a few big pores with secondary vesicles in the walls of these pores. The collapse of particles pyrolyzed at 10 °C/s up to 700 °C we observed in the videotapes is the reason for the flat side often seen in these cross-sections. Under these conditions, the particles were so fluid that they took the shape of the bottom of the pan. Changes in HTT do not seem to have a dramatic effect on the general characteristics of pores both at a heating rate of 1°C/s and 10 °C/s (Figures 4.2).

When the pyrolysis takes place in the presence of oxygen (Figures 4.3 and 4.4), the macropore walls become even thinner. Many char particles produced under these conditions are of the balloon type with one big pore and a few secondary vesicles in the thin wall. The eruptions of internal matter observed in the videotapes during pyrolysis are the cause for the protuberances that can be seen on the cross-sections of Figure 4.4.

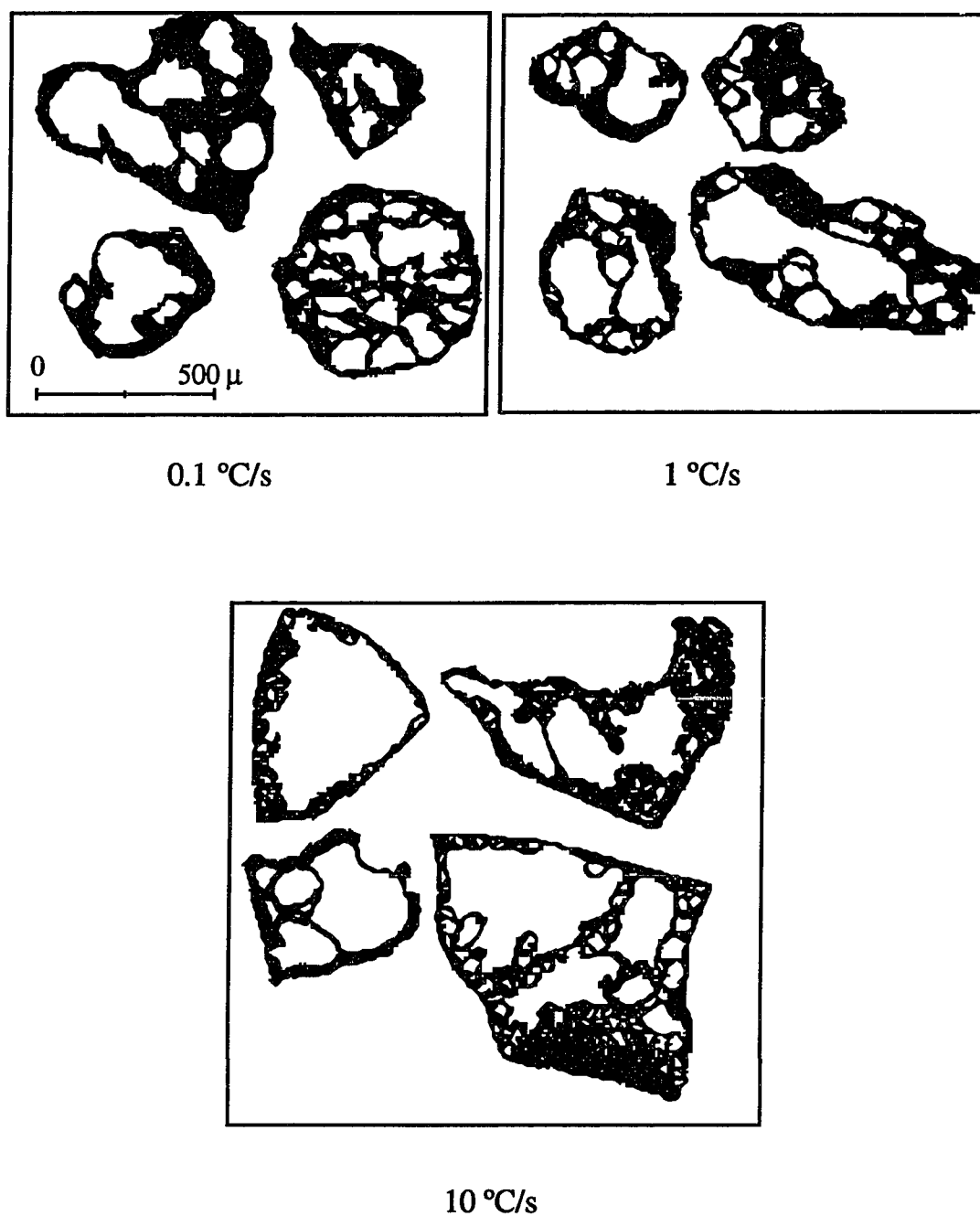
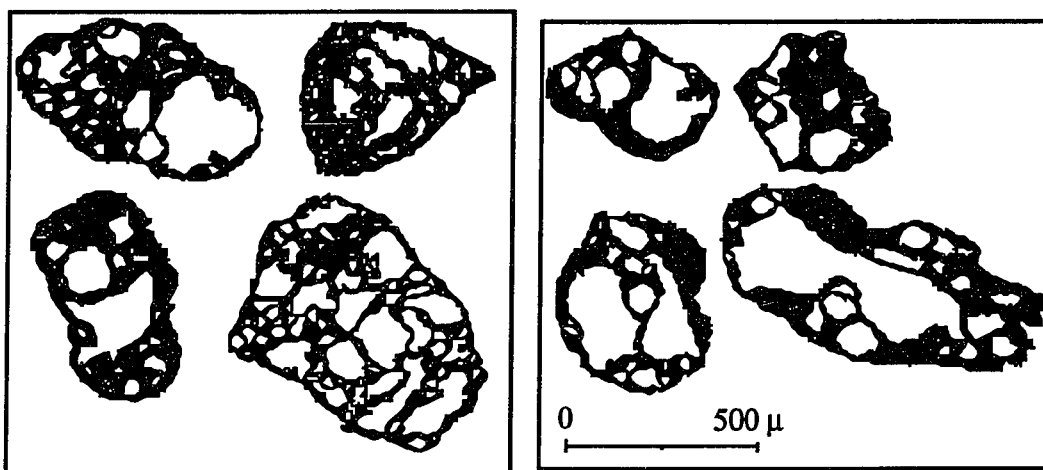
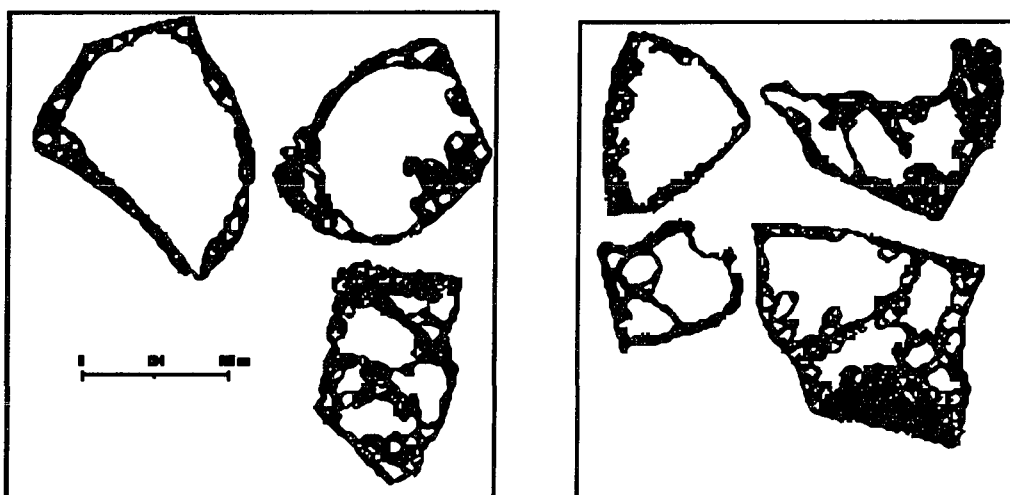


Figure 4.1: Cross sections of particles pyrolysed to an HTT of 700 °C without oxygen



1 °C/s HTT 500°C

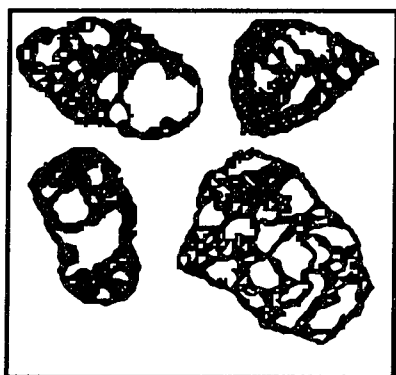
1 °C/s HTT 700 °C



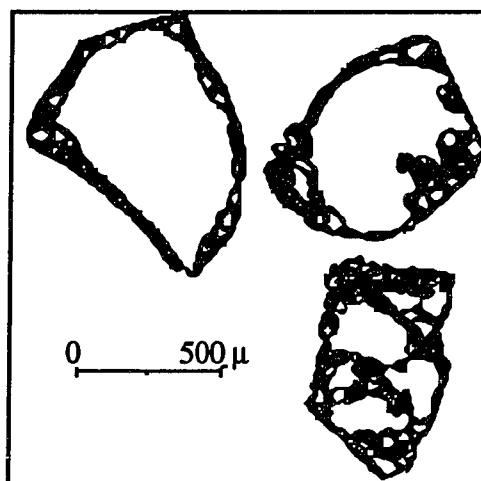
10 °C/s HTT 500°C

10 °C/s HTT 700 °C

Figure 4.2: Cross-sections of particles pyrolysed at 1 °C/s and 10 °C/s without oxygen



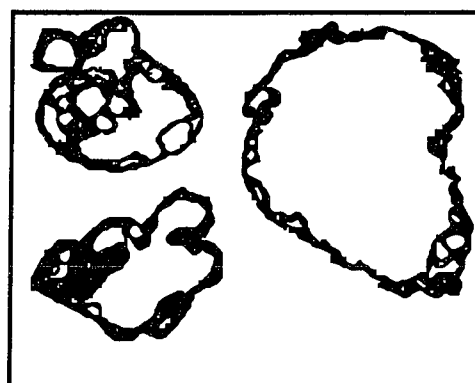
1 °C/s no oxygen



10 °C/s no oxygen

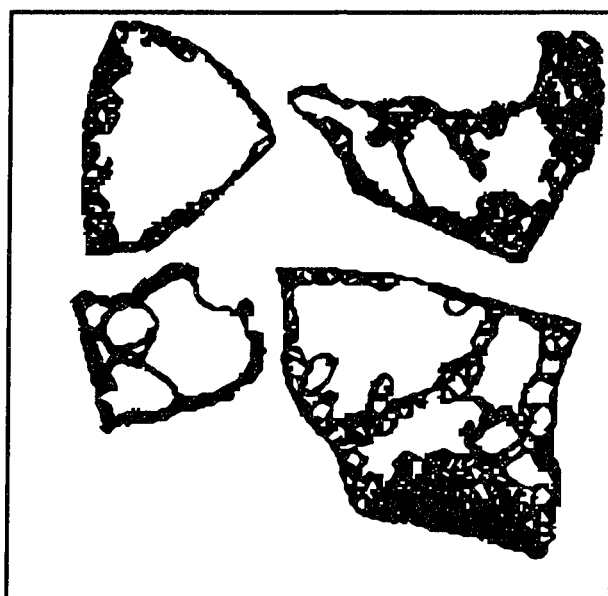


1 °C/s 5% oxygen

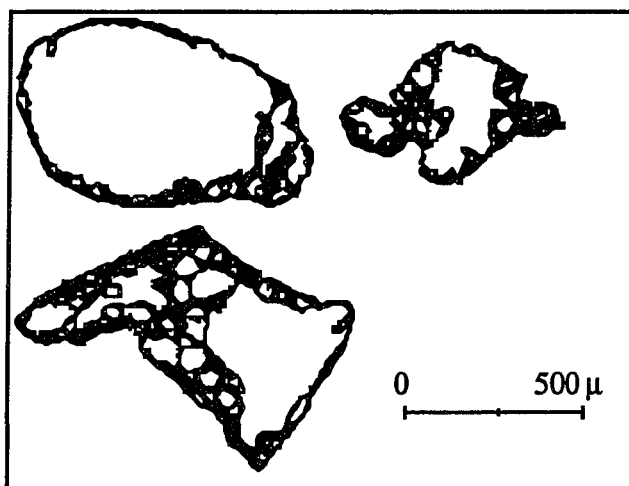


10 °C/s 5% oxygen

Figure 4.3: Cross-sections of particles pyrolysed at 1 °C/s and 10 °C/s at HTT of 500 °C



10 °C/s no oxygen



10 °C/s 5% oxygen

Figure 4.4: Cross-sections of particles pyrolysed at 1 °C/s and 10 °C/s at HTT of 700 °C

4.2 MACROPOROSITY

The greyscale image of each particle cross-section was processed according to the procedure described in Section 2.3.3 to obtain two binary images: one with all the macropore profiles and a second one with the particle cross-section itself. Area, perimeter, pseudo-radius, length, throat and shape factor were computed and stored for each object (pore or section). The size of each sample has been calculated using the method described in Section 2.2. to limit the error to 0.03 with a confidence of 90%. Using the formulas (Weibel, 1980) described in Section 2.4.1, unbiased estimates of the macroporosity were estimated from these data.

These results are given in Table 4.1 and Figure 4.5. For an HTT of 700 °C, there is almost no difference in the value of macroporosity when the heating rate increases from 0.1 °C/s to 1 °C/s. When the pyrolysis heating rate reaches 10 °C/s, however, the measured macroporosity jumped from approximately 0.59 to 0.65 for a relative increase of 9%. For an HTT of 500 °C, the macroporosity increased from 0.57 to 0.67 when the pyrolysis heating rate was raised from 1 °C/s to 10 °C/s (relative increase of over 18%).

The presence of oxygen in the pyrolysis atmosphere also had a significant effect on macroporosity. At a heating rate of 1 °C/s and an HTT of 500 °C, the presence of 5% oxygen in the reactor's atmosphere slightly increased the macroporosity from about 0.57 to about 0.59 (relative change approximately 3%). At a heating rate of 10 °C/s and an HTT of 500 °C, oxygen did not appear to have an appreciable effect on

macroporosity. Note that particle bubbling is not over when the pyrolysis runs end at an HTT of 500 °C for a 10 °C/s heating rate. As a result, some particles may have been contracting when the experiment ended while other may have been expanding. This introduces uncertainty and variability among particles in the determination of macropore structure properties. When the HTT was raised to 700 °C, however, char particles produced at 10 °C/s in the presence of 5% oxygen had considerably higher macroporosity than particles produced in inert atmosphere under the same conditions. The presence of oxygen raised the macroporosity from 0.65 to 0.715 (relative increase over 10%). This is quite logical since the presence of 5% of oxygen affects the plasticity of the coal (Section 3.1). At the high heating rate of 10 °C/s, therefore, most of the structural transformations occurring during the plastic phase will take place when the reactor temperatures exceeds 500 °C.

It is interesting to note that at a heating rate of 1 °C/s, an increase in the HTT from 500 to 700 °C results in an increase in macroporosity of chars produced in inert atmosphere. At 10 °C/s, however, the same increase in HTT results in a drop in the macroporosity. This may be due to the "collapse" and spreading of many particles when they are heated at 10 °C/s up to 700 °C.

Heating Rate°C/s	%O ₂	HTT °C	Macroporosity	S _g cm ² /cm ³	Pyrolysis Weight Loss	S _v cm ² /g
0.1	0	700	0.592 ±0.03	353 ±30	0.3552	702
1	0	500	0.568 ±0.03	530 ±50	0.3365	1210
1	0	700	0.595 ±0.025	504 ±40	0.3812	1127
1	5	500	0.586 ±0.035	507 ±50	0.3290	1116
10	0	500	0.670 ±0.03	394 ±50	0.3663	1452
10	0	700	0.648 ±0.025	366 ±30	0.4255	1731
10	5	500	0.677 ±0.03	389 ±30	0.3504	2150
10	5	700	0.715 ±0.03	357 ±40	0.4247	2032

table 4.1: Unbiased estimates from the 2D results

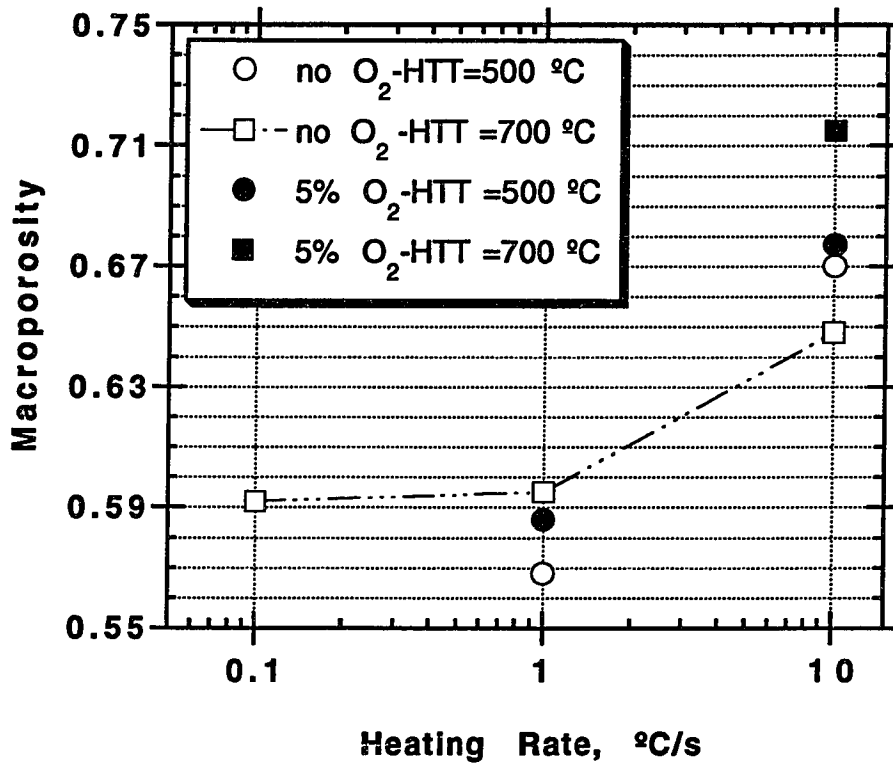


Figure 4.5: Effect of pyrolysis heating rate on macroporosity for two values of heat treatment temperature and two pyrolysis atmospheres.

4.3 MACROPORE SURFACE AREA

The formula proposed by Weibel (Weibel, 1980) and discussed in Section 2.4.1 provides an unbiased estimate of the macropore surface area density, S_V , that can be expressed in unit area of pore exterior surface area per unit volume of particle. Again, the sample sizes were large enough (see

discussion in Section 2.2) to obtain an error smaller than 5 mm² of pore surface area per mm³ of particle with a confidence of 90%.

Table 4.1 presents the computed macropore surface densities in mm² of pore surface area per mm³ of particle. The changes in macropore surface density seem to be depending only on pyrolysis heating rate, with values around 350 cm²/cm³ at 0.1 °C/s, in the lower 500s at 1 °C/s and in the upper 300s for 10 °C/s. These values did not change with HTT or with the composition of the pyrolysis atmosphere.

The specific macropore surface area S_g (expressed in cm² per gram of solid) were computed using data on particle weight loss obtained by independent pyrolysis experiments in our laboratory using the same Illinois #6 coal. The presence of oxygen had little effect on total weight loss (Matzakos, 1991) that increased by less than 20 % when heating rate were raised from 0.1 °C/s to 10 °C/s. The following formula was used to calculate S_g :

$$S_g = S_v \cdot \frac{4}{3} \pi R^3 \cdot \frac{1}{(1 - \alpha)m_0}$$

where R is the average area-equivalent radius for each set of pyrolysis conditions (from Table 3.2), m_0 the average particle weight before pyrolysis ($m_0 = 0.104$ mg for particles in the 28-32 mesh range) and α is the total weight loss at the end of pyrolysis.

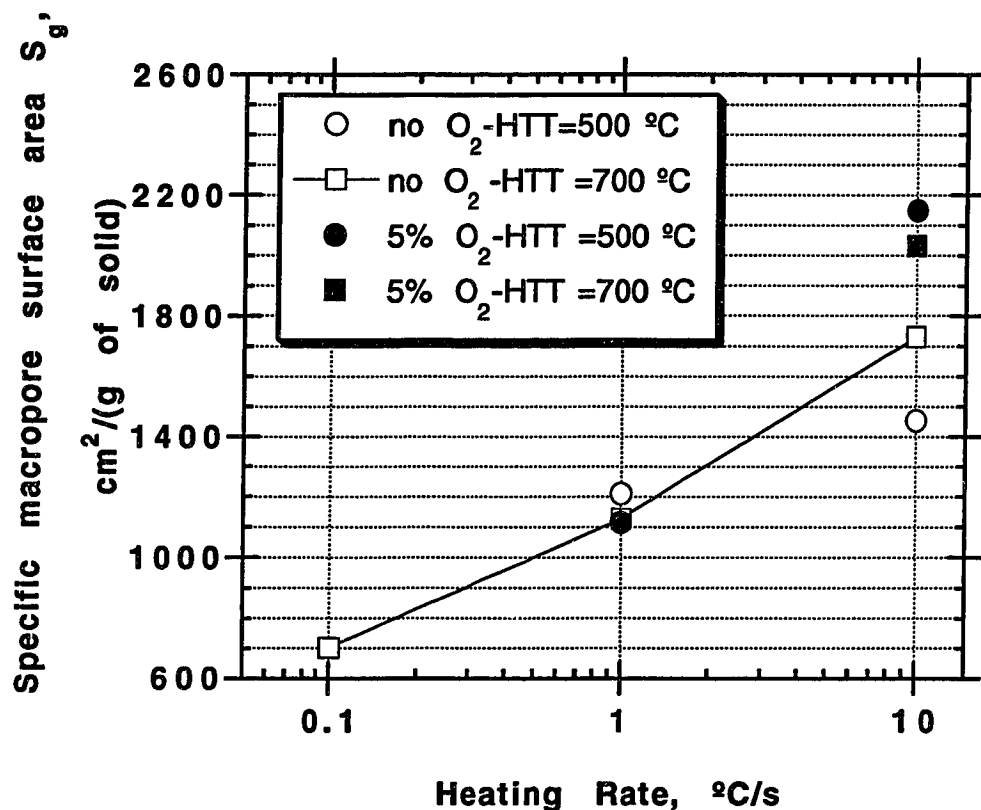


Figure 4.6: Effect of pyrolysis conditions on specific macropore surface area, S_g .

As shown in Figure 4.6, increases in pyrolysis heating rate had a large effect on the specific macropore surface area S_g (per gram of solid). For an HTT of 700 °C, S_g increased by 60% when the heating rate went from 0.1 °C/s to 1 °C/s and increased again by 54% when the heating rate reached 10 °C/s. In the presence of 5% oxygen and for an HTT of 500 °C, S_g increased by 93% when the pyrolysis heating rate went from 1 to 10 °C/s. A smaller increase (20%) in S_g was observed for inert atmosphere

and an HTT of 500 °C when the pyrolysis heating rate went from 1 to 10 °C/s.

All other conditions being equal, changes in HTT do not affect the specific macropore area S_g the same way. In inert atmosphere and at heating rates of 1 °C/s and 10 °C/s, S_g decreases by 9% and increases by 19% respectively when the HTT is raised from 500 to 700 °C. At 10 °C/s with 5% of oxygen, S_g decreased by 5% when the HTT was raised from 500 to 700 °C.

The presence of oxygen in the reactor's atmosphere did not significantly affect the specific macropore surface area S_g at a heating rate of 1 °C/s. At a heating rate of 10 °C/s with HTT's of 700 °C and 500 °C, the presence of oxygen increased S_g by 17% and 48% respectively.

4.4 PORE SIZE DISTRIBUTION

For each set of pyrolysis parameters, more than 2000 pore cross-sections were analyzed to obtain the size distribution of three-dimensional pores using the stereological method described in Section 2.4.2.

The histograms describing these distributions are presented on Figures 4.7 and 4.8. Volume distribution data are given in these figures because even though large pores are very few they account for a large fraction of the total macroporosity. It is easier to analyze the changes in pore distribution by studying the cumulative curves representing the fraction of macropore volume attributable to macropores of a given size. These curves are represented on Figures 4.9 to 4.12.

To simplify the following discussion, we will divide the macropores into the following four classes.

- A. Macropores with area-equivalent radii smaller than 0.05 mm.
- B. Macropores with area-equivalent radius between 0.05 mm and 0.15 mm.
- C. Macropores with area-equivalent radius between 0.15 mm and 0.25 mm;
- D. Macropores with area-equivalent radius larger than 0.25 mm.

Let us also define R50 as the radius at the middle of the macropore volume cumulative distribution. Thus, 50% of the macropore volume is associated with macropores with radius smaller than R50. The values of R50 are presented in table 4.2.

Table 4.2
Values of R50

heating rate °C/s	% O ₂	HTT °C	R50 mm	heating rate °C/s	% O ₂	HTT °C	R50 mm
0.1	0	700	0.12	10	0	500	0.20
1	0	500	0.055	10	0	700	0.19
1	0	700	0.13	10	5	500	0.14
1	5	500	0.075	10	5	700	0.25

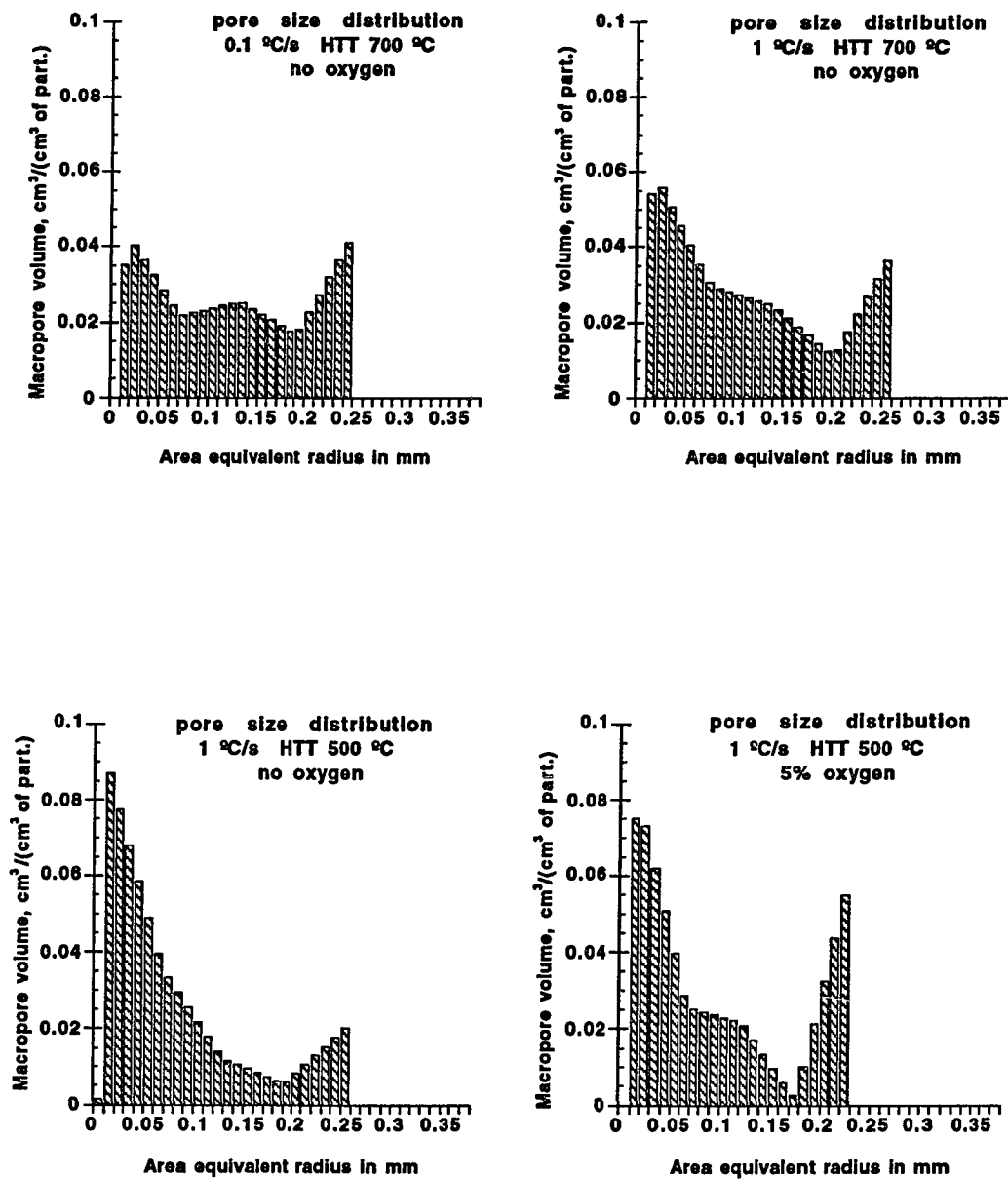


Figure 4.7: Macropore distribution for heating rates of 0.1 °C/s and 1 °C/s.

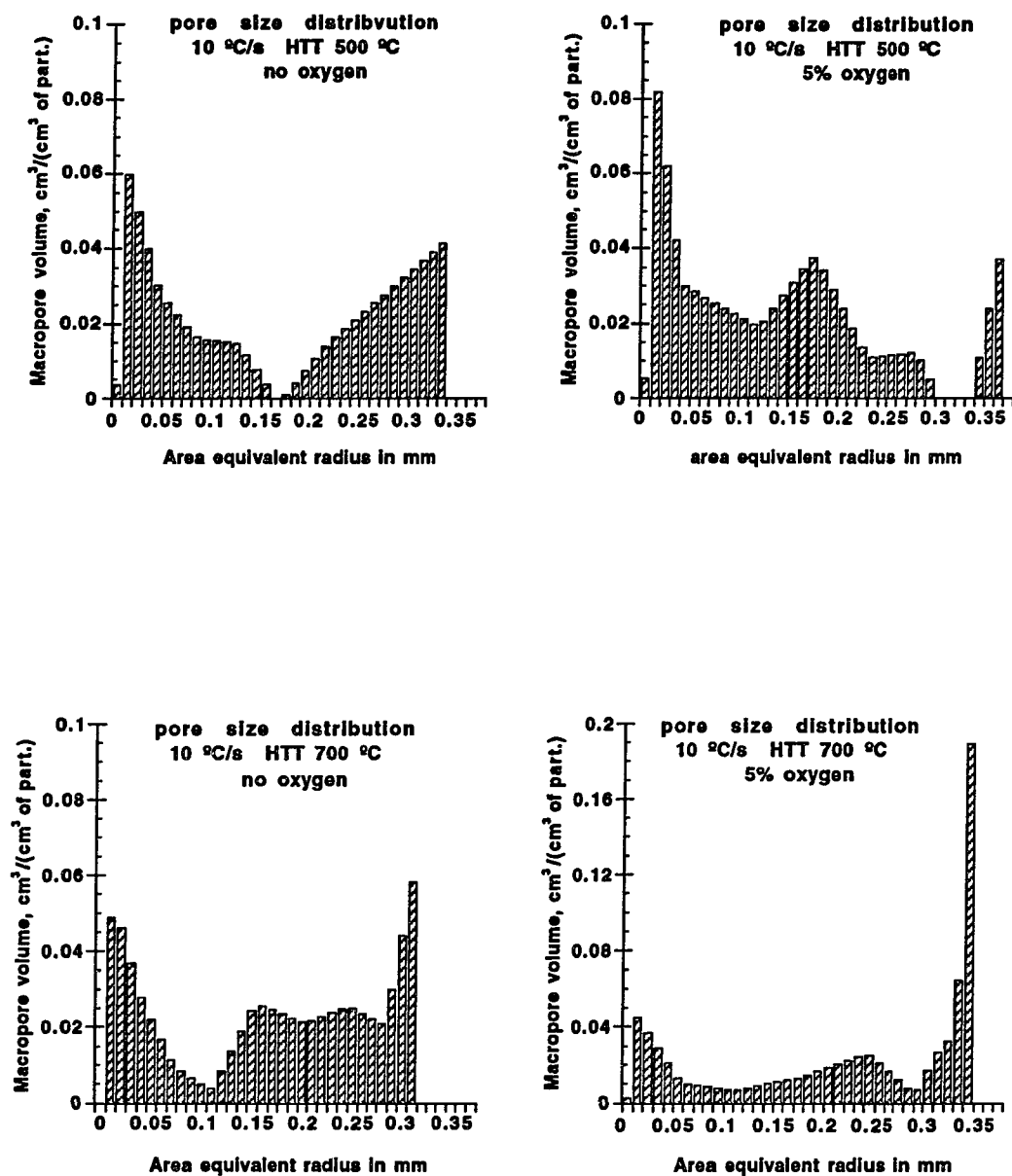


Figure 4.8: Macropore size distribution for heating rate of 10 °C/s

The change of heating rate from 0.1 °C/s to 1 °C/s did not significantly affect either the pore size distribution or R50. The only noticeable difference in the two distributions is an increase in the volume attributed to the small macropores of class A (Figure 4.7). Larger macropores of class D appeared in char particles pyrolyzed at 10 °C/s with the two different HTTs (Figure 4.8). This is the reason why R50 for these distributions increased to about 0.2 mm from 0.1 mm. These large macropores account for most of the macropore volume (Figure 4.9). The total macropore volume associated with pores in classes A, B and C did not change (Figures 4.7 and 4.8) with heating rate. The fraction of macropore volume coming from each class, however, is not the same. At an HTT of 700 °C in inert atmosphere and 500 °C in reactive atmosphere, there is a transfer from class B to class C, while with an HTT of 500 °C in inert atmosphere, there is transfer from class A to classes B and C.

The value of the final pyrolysis temperature affects the pore size distribution more than any of the other structural parameters we have studied before. In inert atmosphere and an HTT of 500 °C, most of the macropore volume comes from the smallest and the biggest pores. That is from classes A and C for a heating rate of 1 °C/s (Figure 4.7) and classes A and D for 10 °C/s (Figure 4.8). An increase in HTT from 500 to 700 °C induces the appearance of pores of medium size and a decrease of the volume of pores of class A (Figure 4.10).

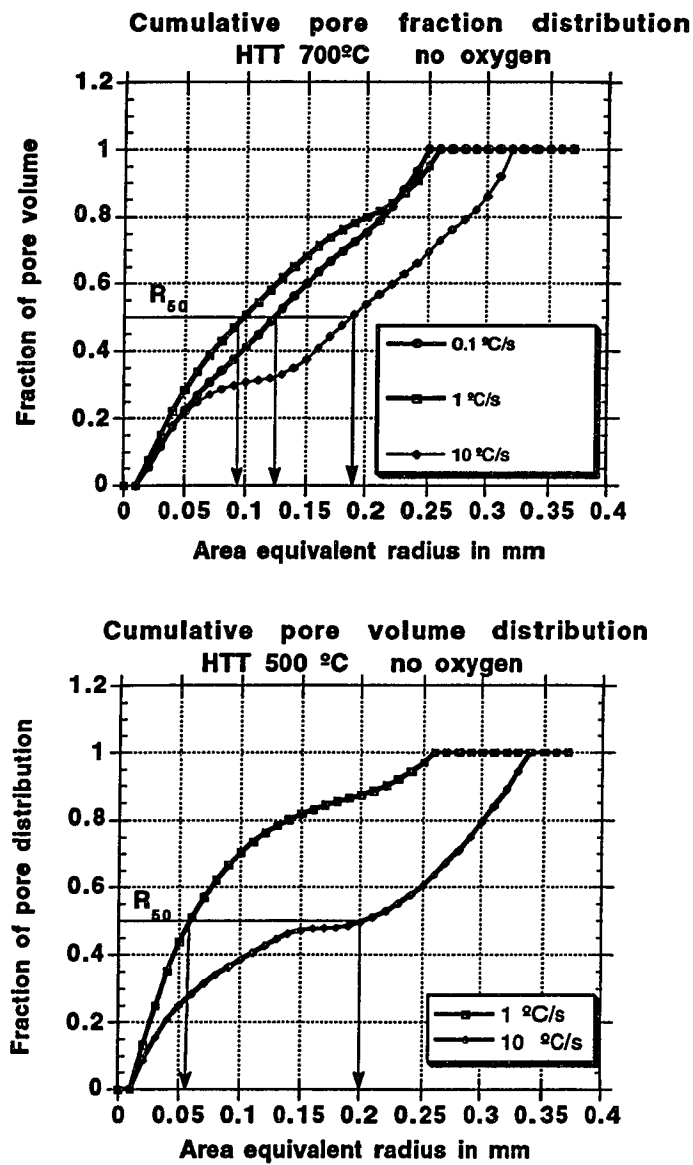


Figure 4.9: Effect of pyrolysis heating rate on macropore volume distribution.

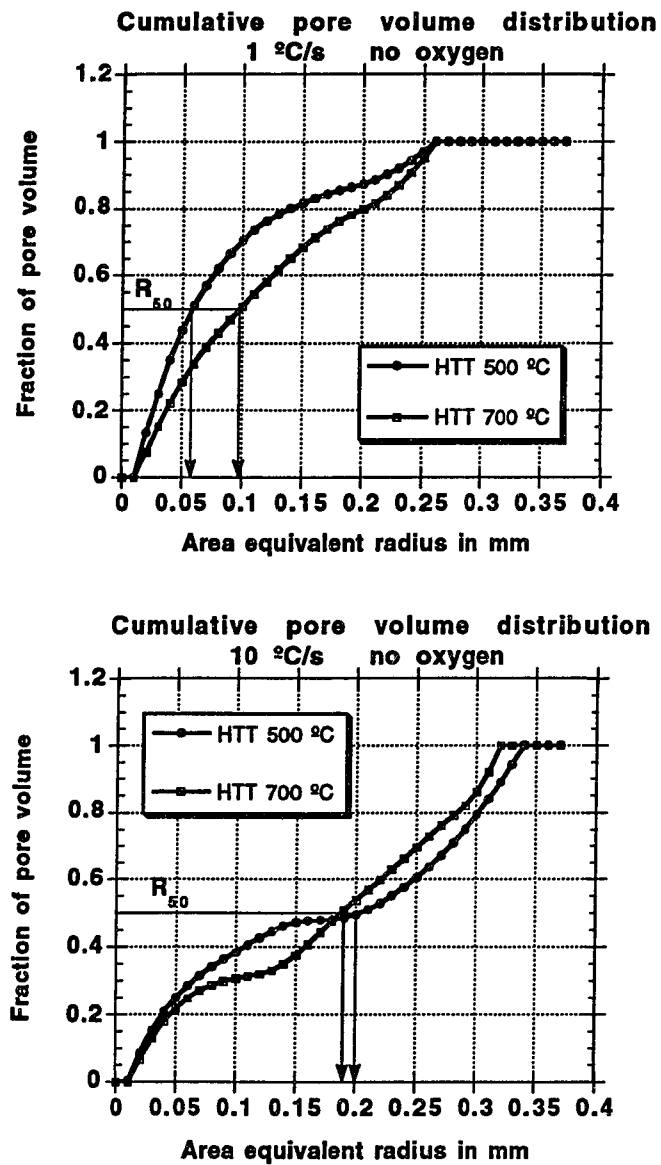


Figure 4.10: Effect of heat treatment temperature on macropore volume distribution.

The presence of 5% of oxygen in the pyrolysis atmosphere does not have a strong effect on the value of R_{50} (Figures 4.11 and 4.12). At 1 °C/s and HTT of 500 °C, the distribution is almost the same. At 10 °C/s, the number of medium pores, of class C increases for HTT of 500 °C (figure 4.12) and bigger pore appear (Figures 4.8 and 4.12).

From these distributions we computed the values of porosity and surface area density using the mid-bin value of the area-equivalent radius. These results are presented in Table 4.3. The computed structural properties are different from the unbiased estimates obtained from the cross-sections (Figures 4.13 and 4.14). Macroporosities are higher and surface area densities are smaller than the unbiased estimates computed before. However, the qualitative trends we observed for the different pyrolysis conditions in Sections 4.2 and 4.3 are still valid.

Differences between the two methods are due to the limitations of the stereological method that represents pores as non-overlapping spheres. Since real pores are not smooth spheres (as it can be seen in Figures 4.1 to 4.4), the stereological method computes lower surface area densities. Also, the macropores are connected (we can represent them as overlapping volumes) and this is why the stereological method overestimates the macroporosity. A better stereological method would consider overlapping non-spherical (maybe ellipsoidal) pores, but this approach would require large sets of data to obtain statistically representative samples.

Heating Rate °C/s	O ₂ %	HTT °C	Macro- porosity	S _v cm ² /cm ³	S _g cm ² /g
0.1	0	700	0.654	290	577
1	0	500	0.667	485	1107
1	0	700	0.700	383	856
1	5	500	0.678	436	960
10	0	500	0.734	357	1316
10	0	700	0.733	303	1433
10	5	500	0.827	357	1973
10	5	700	0.797	281	1599

Table 4.3: porosity and surface area density from pore distribution

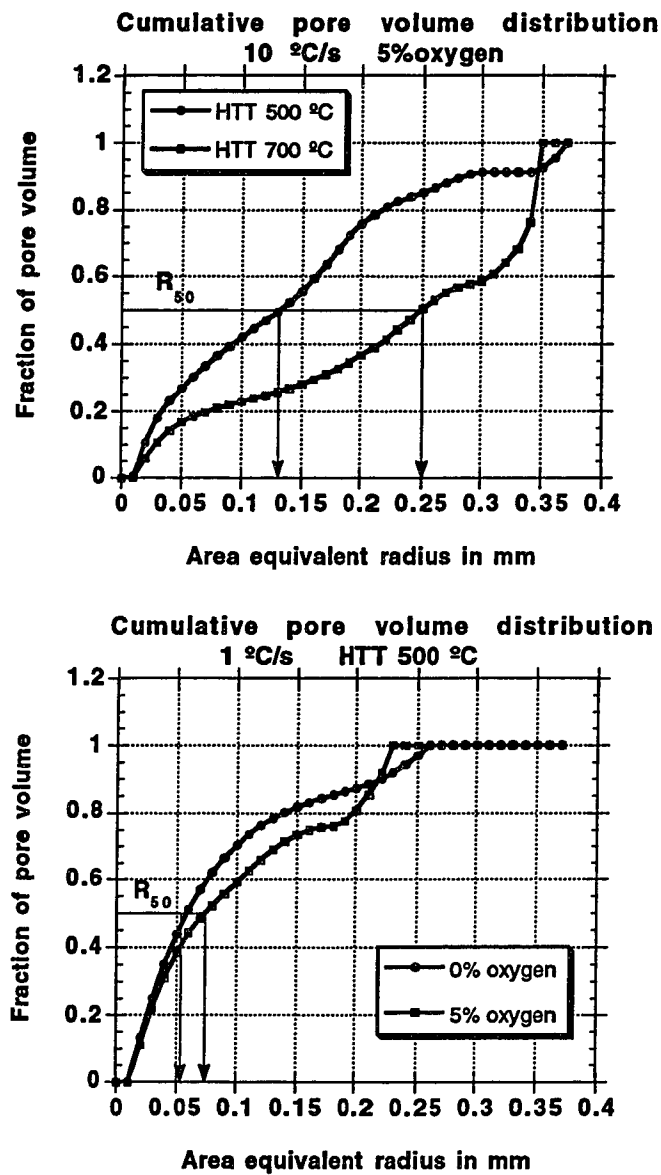


Figure 4.11: Effect of heat treatment temperature (HTT) and oxygen on macropore volume distribution.

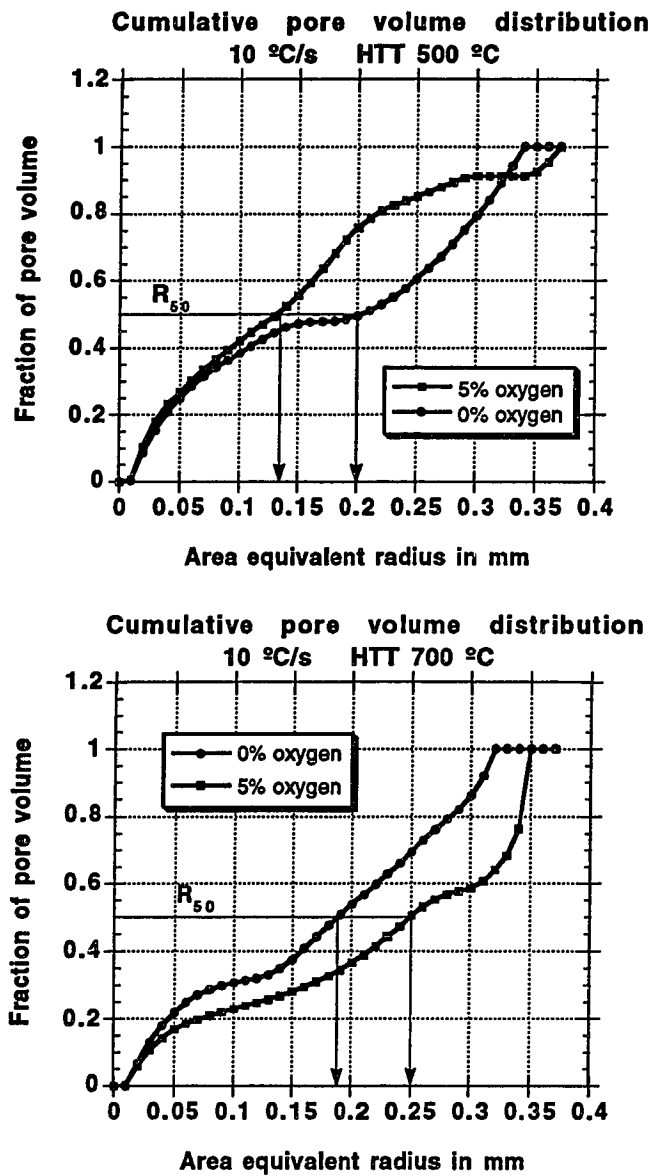


Figure 4.12: Effect of oxygen on macropore size distribution.

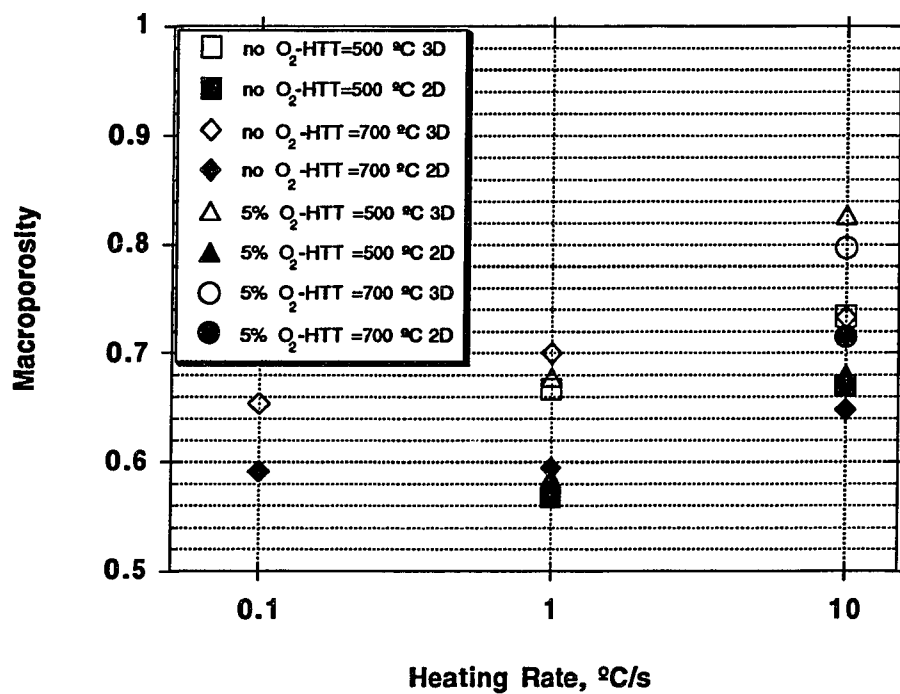


Figure 4.13: Differences in macroporosity between the unbiased estimate and the value given by the stereological method

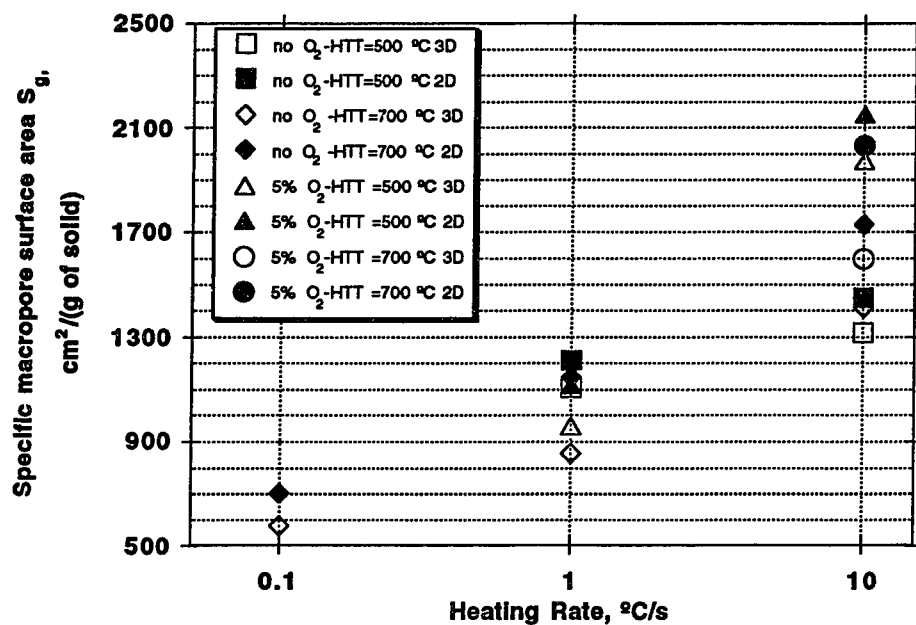


Figure 4.14: Differences in specific macropore surface area between the unbiased estimate and the value given by the stereological method

CHAPTER 5 CONCLUSIONS AND RECOMMENDATIONS FOR FUTURE WORK

5.1 MACROPORE STRUCTURE AND CHAR REACTIVITY DURING COMBUSTION

The effects of the pyrolysis conditions on char combustion have been previously studied in our laboratory (Matzakos, 1991) and Section 1.3.1 presented a short description of this work. In the following section, we will analyze Matzakos' conclusions using the results from the current study.

5.1.1 Effect of HTT on Char Reactivity

Matzakos' study showed that the reactivity of chars during combustion at low temperatures (450 °C) decreases with increasing HTT. Since at such low temperatures chars react in the kinetic control regime, an increase in HTT implies a decrease in intrinsic reactivity. Changes in intrinsic reactivity tend to screen the effect of HTT on reactivity in the diffusion limited regime. We showed in the previous sections that changing HTT from 700 °C to 500 °C, all other pyrolysis parameters being constant,

changes the average size of the particle (section 4.1.2.4.), the porosity (section 4.2.2.1.) or the macropore surface area (section 4.2.2.2.). These changes have no general trend and depend on the values of the other parameters. Anyway, it is interesting to see that the value of HTT has some influence on the structure of char particles.

5.1.2 Effect of heating rate

When combustion takes place in the kinetic control regime, pyrolysis heating rates do not affect the reactivity of chars indicating that the micropore structure and intrinsic reactivity of chars do not depend on the pyrolysis heating rate. When reacted in the regime of diffusional limitations, however, chars produced at high pyrolysis heating rates exhibited higher reactivity and lower ignition temperatures than chars produced at low pyrolysis heating rates [Matzakos A., 1991 #25].

Our results agree with the combustion data obtained in our laboratory. When the pyrolysis heating rate is increased from 0.1 °C/s to 10 °C/s, we showed that the particles swell more (Section 4.1.2.3.), larger macropores are formed (Section 4.2.2.3.) and the macroporosity (section 4.2.2.1.) and macropore specific surface area increase (Section 4.2.2.2.). Thus, char particles produced at high pyrolysis heating rates have more open macropore network that significantly decreases diffusional limitations during combustion. The larger macropores are more accessible, the concentration of the gaseous reactants is higher inside the particle and consequently the reaction rate is enhanced. Higher porosity, larger particle

size and lower macropore diffusional limitations are three possible justifications of lower ignition temperature.

5.1.3 Effect of oxygen

With the study of combustion reaction rates in the chemical control regime, Matzakos proved that the presence of oxygen during pyrolysis does not alter the micropore structure and intrinsic reactivity of chars. During combustion in the diffusion limited regime, however, he observed reactivity patterns with sharp maxima caused by ignitions for particles pyrolyzed at 10 °C/s in a reactive atmosphere (5% oxygen). This behavior, that does not appear for pyrolysis at 1 °C/s, can be explained by our results on the porous structure of particles produced under those conditions: larger particles with higher porosity and larger surface area available to reaction (Sections 4.1.2.5., 4.2.2.1. and 4.2.2.2.).

5.2 CONCLUSIONS

The main contribution of this study is the systematic analysis of the pore structure of chars produced from an Illinois #6 under a variety of pyrolysis conditions. An extensive set of reactivity data for these chars existed in our laboratory.

We carried out detailed measurements to characterize the char particle size, macroporosity, specific macropore surface area (per unit mass of solid) and an approximate macropore size distribution. Our data confirm

the strong correlation of pyrolysis conditions and char reactivity in the diffusion limited regime that has been presented by Matzakos (Matzakos, 1991). Our data can also provide the necessary parameters for models describing combustion of chars in the diffusion limited regime.

We observed the effect of three parameters of pyrolysis:

- **Heat Treatment Temperature:** The change of HTT from 700 °C to 500 °C has some effect on macropore structure of Illinois #6 particles. These effects have no general trend but are not negligible.
- **Pyrolysis Heating Rate:** By increasing the heating rate from 1 to 10 °C/s, we produced much bigger char particles with higher macroporosity (about 65%) and macropore surface area (around 1500 cm²/g).
- **Composition of Pyrolysis Atmosphere:** When 5% of oxygen (quantity small enough to prevent any reaction during the pyrolysis phase) is present in the pyrolysis atmosphere, we have larger swelling, higher macroporosity (up to 70%) with specific macropore surface area of more than 2000 cm²/g.

These results are necessary to choose the values of the pyrolysis parameters in order to produce more reactive char particles, optimize the efficiency of combustion processes and make the combustion stage more efficient in terms of energy utilization, emission control and heat production rates.

5.3 RECOMMENDATIONS FOR FUTURE WORK

The image analysis method proposed in this study, is not limited to the pyrolysis conditions that we used. Different elements should be explored:

- Particles of a variety of coals should be studied. In particular, coals that are less plastic might exhibit important changes in their pore structure, even when particles do not appear to change significantly.
- Additional pyrolysis and system parameters (e.g. coal particle size and soak time) should be studied in detail.
- The range of the parameters studied should be expanded. For example, higher heating rates could be used. Very high heating rates may degrade the performance of our temperature control algorithm. Currently, our digital controller is accurate enough to pyrolyze particles at a rate of 20 °C/s in the TGA/VMI reactor. Its performance for high heating rates in the hot-stage reactor should be studied.
- It would be interesting to determine if there is an optimum concentration of oxygen in the pyrolysis reactor to obtain the biggest particles possible without appreciable combustion.
- By following the size of particles during pyrolysis, it should be possible to determine the values of HTT at which we could stop pyrolysis to obtain particles with different characteristics. These values of HTT will depend on the heating rate since different heating rates have different ranges for coal plasticity.

- The determination of the pore size distribution should be improved. The fact that pores are overlapping should be taken into account first. We should also relax the assumption that macropores are spherical by considering, for example, ellipsoidal pores.
- It would be interesting to distinguish pores that are filled by the resin and those that are not. The surface area of pores that have not been filled with resin will not be accessible to reaction in the initial stages. These macropores will become accessible to reactants when the reaction front reaches them by creating openings in pore walls. This is quite important for the modeling of char combustion.

REFERENCES

Ballal, G. and K. Zygourakis. (1987). Ind. Eng. Chem. Research. **26**(5): 911-921.

Berkowitz, N. (1979). "Environment aspects of coal utilization." In An introduction to coal technology, Academic Press Ed..

Berkowitz, N. (1985). "The chemistry of coal." In Coal Science and Technology, Elsevier Ed..

Birch, T., K. Hall and R. Urie. (1960). J. Inst. Fuel. **33**: 422-435.

Bond, R. and F. Maggs. (1949). Fuel. **28**: 172-175.

Bouska, V. (1981). Geochemistry of coal. , Elsevier Ed..

Chen, M., L. Fan and R. Essenhigh. (1984). Proc. 20th Symposium on Combustion. : 1513-1521.

Comité Professionnel du Pétrole. (1989). "Statistiques pétrolières et énergétiques 1988." Comité Professionnel du pétrole Report.

de Hoff, R. (1983). J. Microsc. **131**(3): 259-263.

Dulhunty, J. and B. Harrison. (1953). Fuel. **32**: 441-450.

Durif, S. (1963). J. Chim.Phys. **60**: 816-824.

Eavenson, H. (1939). Coal through the ages. , A.I.M.E. Ed..

Forney, A., R. Kenny and S. Gasior. (1964). I&EC Prod Res Dev. **3**: 48-53.

Gavalas, G. (1980). AICHE J. 26(4): 577-585.

Given, P., M. Peover and W. Wyss. (1960). Fuel. 39: 323-340.

Glass, M. (1987). Stereological analysis of the macropore structure of chars produced under various pyrolysis conditions and the influence of macropore structure on char gasification rates in the presence of strong diffusional limitations. PhD Dissertation, Rice University.

Glass, M. and K. Zygourakis. (1988). Rev. Sci. Instrum. 59(4): 580-587.

Grainger, L. and G. J. (1981). Coal Utilization: Technology, Economics and Policy. , Halsted Press Ed..

Grimes, W. (1982). "The physical structure of coal." In Coal science, Ed..

Hamilton, L. (1980). Fuel. 59: 221-226.

Hessley, R. and J. Reasoner. (1986). Coal Science, an introduction to coal chemistry and utilization. , Wiley Ed..

Hildebrand, D. (1986). "Statistical inference: estimation section 8.4: determining the sample size." In Statistical thinking for behavioral scientists, Duxbury Press Ed..

Howard, H. (1963). "Pyrolytic Reactions of Coal." In Chemistry of coal utilization, Wiley Ed..

IUPAC. (1972). Manual of Symbols and Terminology for Physico Chemical Quantities and Units. , Ed..

Judkins, R., W. Fulkerson and M. Sanghvi. (1991). Prep ACS Div. Fuel Chem. 36(1): 331-343.

Loison, R., A. Peytavy and A. Boyer. (1963). "The plastic properties of coal." In Chemistry of coal utilization, Wiley Ed..

Lowell Miller, C. (1990). Prep. ACS Div. Fuel Chem. **35**(4): 1358-1372.

Mackowsky, M. and E. Wolf. (1965). Microscopic investigation of pore formation during coking. Advances in chemistry. 527-548.

Mahajan, O. (1982). "Coal Porosity." In Coal Structure, Academic Press Ed..

Mahajan, O., M. Komatsu and P. Walker. (1980). Fuel. **59**: 3-10.

Matzakos, A. (1991). Fundamental mechanisms of coal pyrolysis and char combustion. PhD Dissertation, Rice University.

Matzakos, A. and K. Zygourakis. (1990). Prep. ACS Div. Fuel Chem. **35**(2): 505-515.

Moseley, F. and D. Paterson. (1965). J. Inst. Fuel. **38**: 13-23.

Neavel, R. (1982). "Coal plasticity mechanism: inferences from liquefaction studies." In Coal science, Academic Press Ed..

Nelson, J., O. Mahajan and P. Walken. (1980). Fuel. **59**: 831-837.

Oh, M., J. Howard and W. Peters. (1984). "Modeling volatiles transport in softening coal pyrolysis." Procs. AIChE annual meeting, pp.

Rouzaud, J. and A. Oberlin. (1990). "The characterization of coals and cokes by transmission electron microscopy." In Advanced Methodology in Coal Characterization, Elsevier Ed..

Shell Chemical Company. (1990). Epon Resin Structural Reference Manual.

Sinnatt, F., A. McCulloch and H. Newall. (1927). J. Soc. Chem. Ind. (46): 331-335.

Sotirchos, S. and N. Amundson. (1984). Ind. Eng. Chem. Fundam. **23**: 191-201.

Speight, J. (1983). The chemistry and technology of coal. , Marcel Dekker Ed..

Stack, E., M. T. Mackowsky and M. Teichmuller. (1975). Coal Petrology. , Borntraeger Ed..

Street, P., R. Weight and P. Lightman. (1968). Fuel. **47**: 343-364.

van Krevelen, D. (1961). Coal : typology, chemistry, physics, constitution. , Elsevier Ed..

Vorres, K. (1990). Energy & Fuels. **4**(5): 420-426.

Weibel, E. (1980). Stereological methods. , Academic press Ed..

Wicksell, S. (1925). Biometrika. **17**: 84-99.

Wiser, W. (1968). Fuel. **47**: 475-485.

Zygourakis, K. (1993). Energy & Fuels. **7**(1): 33-41.

Zygourakis, K. and M. Glass. (1988). Chem. Eng. Comm. **70**: 39-55.

Zygourakis, K. and C. Sandmann. (1988). AIChE Journal. **34**(12): 2030-2040.